Article

Immunity

Lymphocyte Circadian Clocks Control Lymph Node Trafficking and Adaptive Immune Responses

Graphical Abstract

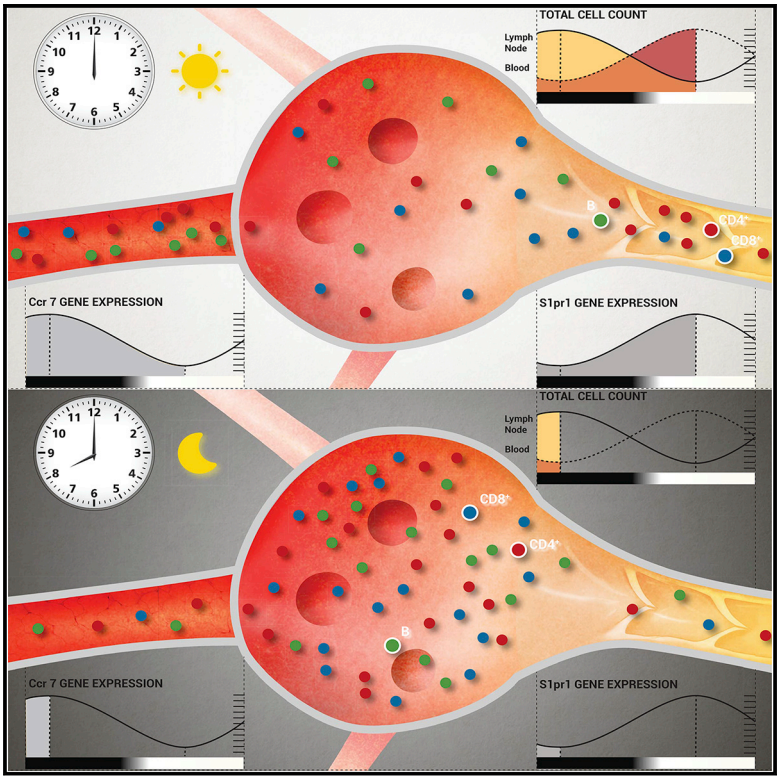

Authors

David Druzd, Olga Matveeva, Louise Ince, ..., Werner Solbach, Henrik Oster, Christoph Scheiermann

Correspondence

christoph.scheiermann@med.uni-muenchen.de

In Brief

Lymphocyte trafficking through lymph nodes and lymph is an important immune surveillance mechanism of the body. Druzd et al. (2017) demonstrate that this trafficking occurs in a circadian manner and that adaptive immune responses are also time-of-day dependent and are ablated when circadian clock function is lost in T cells.

Highlights

- Lymphocyte numbers in lymph nodes and lymph oscillate over the course of the day
- Rhythmic *Ccr7* and *S1pr1* expression drives rhythmic lymphocyte homing and egress
- Adaptive immune responses to immunization and pathogens are time-of-day dependent
- Loss of circadian clocks in lymphocytes ablates rhythmic adaptive immune responses

Druzd et al., 2017, Immunity *46*, 120–132
January 17, 2017
http://dx.doi.org/10.1016/j.immuni.2016.12.011

CellPress

CellPress

Immunity
Article

Lymphocyte Circadian Clocks Control Lymph Node Trafficking and Adaptive Immune Responses

David Druzd,[1,11] Olga Matveeva,[2,11] Louise Ince,[1] Ute Harrison,[3] Wenyan He,[1] Christoph Schmal,[4] Hanspeter Herzel,[5] Anthony H. Tsang,[2] Naoto Kawakami,[6] Alexei Leliavski,[7] Olaf Uhl,[8] Ling Yao,[9] Leif Erik Sander,[9] Chien-Sin Chen,[1] Kerstin Kraus,[1] Alba de Juan,[1] Sophia Martina Hergenhan,[1] Marc Ehlers,[7] Berthold Koletzko,[8] Rainer Haas,[3] Werner Solbach,[10] Henrik Oster,[2] and Christoph Scheiermann[1,12,*]

[1]BioMedical Center, Walter-Brendel-Centre for Experimental Medicine, Ludwig-Maximilians-University, 82152 Planegg-Martinsried, Germany
[2]Medical Department I, University of Lübeck, 23562 Lübeck, Germany
[3]Max von Pettenkofer-Institute for Hygiene and Medical Microbiology, Ludwig-Maximilians-University, 80336 Munich, Germany
[4]Charité University Hospital Berlin, 10117 Berlin, Germany
[5]Institute for Theoretical Biology, Humboldt University of Berlin, 10115 Berlin, Germany
[6]BioMedical Center, Institute of Clinical Neuroimmunology, Ludwig-Maximilians-University, 82152 Planegg-Martinsried, Germany
[7]Laboratory of Immunology, Institute for Nutrition Medicine, University of Lübeck, 23562 Lübeck, Germany
[8]Ludwig-Maximilians-University, Dr. von Hauner Children's Hospital, University of Munich Medical Center, 80337 Munich, Germany
[9]Department of Infectious Diseases and Pulmonary Medicine, Charité University Hospital Berlin, 10117 Berlin, Germany
[10]Center for Infection and Inflammation, University of Lübeck, 23562 Lübeck, Germany
[11]Co-first author
[12]Lead Contact
*Correspondence: christoph.scheiermann@med.uni-muenchen.de
http://dx.doi.org/10.1016/j.immuni.2016.12.011

SUMMARY

Lymphocytes circulate through lymph nodes (LN) in search for antigen in what is believed to be a continuous process. Here, we show that lymphocyte migration through lymph nodes and lymph occurred in a non-continuous, circadian manner. Lymphocyte homing to lymph nodes peaked at night onset, with cells leaving the tissue during the day. This resulted in strong oscillations in lymphocyte cellularity in lymph nodes and efferent lymphatic fluid. Using lineage-specific genetic ablation of circadian clock function, we demonstrated this to be dependent on rhythmic expression of promigratory factors on lymphocytes. Dendritic cell numbers peaked in phase with lymphocytes, with diurnal oscillations being present in disease severity after immunization to induce experimental autoimmune encephalomyelitis (EAE). These rhythms were abolished by genetic disruption of T cell clocks, demonstrating a circadian regulation of lymphocyte migration through lymph nodes with time-of-day of immunization being critical for adaptive immune responses weeks later.

INTRODUCTION

Lymphocytes survey antigen by circulating through blood, lymph nodes (LNs) and lymph and shape specific immune responses in LNs. To enter LNs, lymphocytes must undergo extensive interactions with high endothelial cell venules (HEVs) (Butcher, 1991; Förster et al., 2008; Ley et al., 2007; Muller, 2011; Springer, 1994; Vestweber and Blanks, 1999; von Andrian and Mempel, 2003; Wagner and Frenette, 2008). Lymphocytes initially tether on peripheral nodal addressin (PNAd) expressed on HEVs using L-selectin (CD62L) as a ligand. Lymphocytes roll along the vascular endothelium and become activated via interactions of the chemokine receptors CCR7 and CXCR4 with their respective ligands CCL21 and CXCL12. Activated leukocytes use the integrin LFA-1 (CD11a) to bind to ICAM-1 to promote adhesion and finally emigrate into the LN parenchyma.

After LN entry, lymphocytes interact with dendritic cells in order to scan presented antigen (Gasteiger et al., 2016), and finally emigrate into efferent lymphatic vessels. For this egress, expression of the sphingosine-1-phosphate-receptor 1 (S1P1, encoded by *S1pr1*) on lymphocytes is critical, recognizing the chemoattractant phospholipid sphingosine-1-phosphate (S1P) (Matloubian et al., 2004). S1P concentrations are high in blood and lymph but low in tissues, thus providing a gradient that guides lymphocytes out of the LN and into efferent lymph (Cyster and Schwab, 2012). This mechanism is therapeutically exploited for treating multiple sclerosis patients by antagonizing S1P1 function with the drug FTY720 (fingolimod) to keep autoreactive T cells from exiting LNs and entering the central nervous system (Massberg and von Andrian, 2006).

Lymphocyte trafficking into LNs is believed to occur in a continuous fashion, and not to be influenced by time-of-day variables. Moreover, it is generally unclear whether circadian rhythms regulate overall cellularity in these tissues (Arjona and Sarkar, 2005; Esquifino et al., 1996; Fortier et al., 2011; Hemmers and Rudensky, 2015).

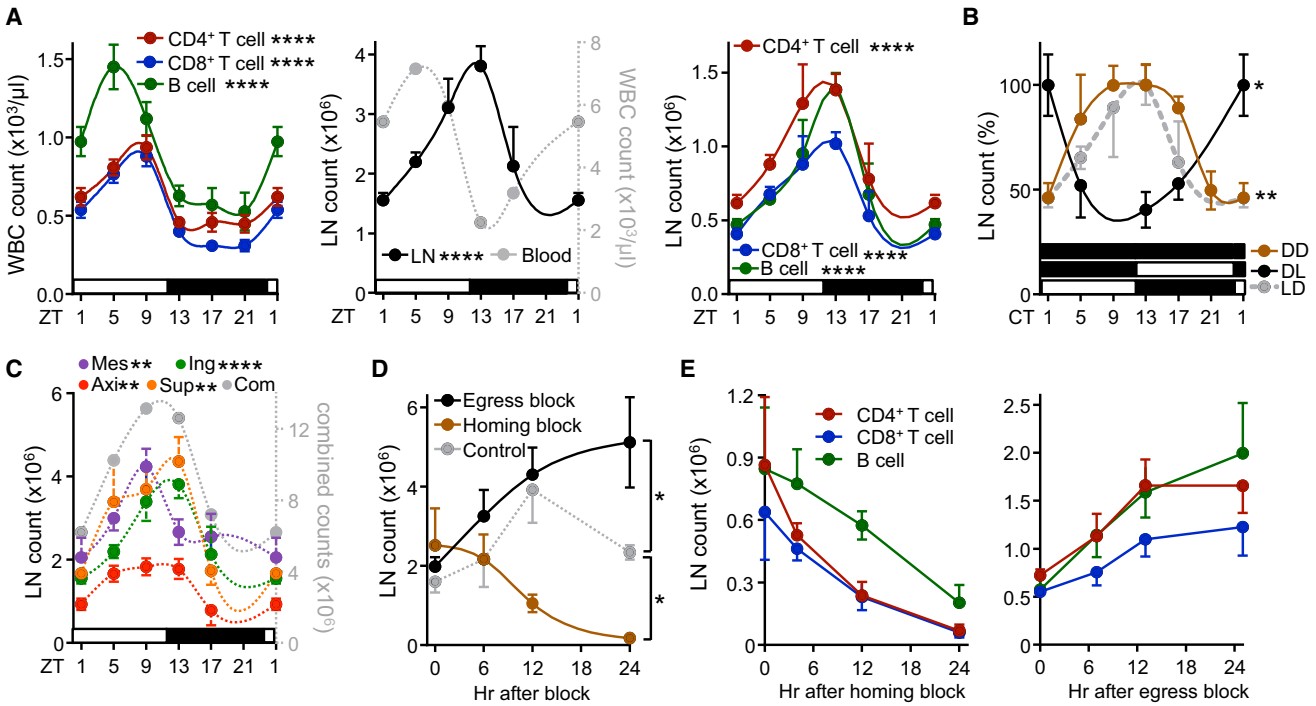

Figure 1. Lymphocyte Numbers Exhibit Circadian Oscillations in Lymph Nodes

(A) Lymphocyte oscillations in blood (left panel) and inguinal lymph node (middle and right panels) over 24 hr. Zeitgeber time (ZT, time after light onset) 1 is double-plotted to facilitate viewing; n = 4–49 mice, one-way ANOVA, WBC: white blood cells.

(B) Lymph node oscillations under light-dark (LD), dark-dark (DD) and inverted, dark-light (DL) conditions, normalized to peak times; CT, circadian time in constant darkness conditions; n = 3–15 mice, one-way ANOVA.

(C) Oscillations across multiple lymph nodes, axi: axillary, sup: superficial cervical, ing: inguinal, mes: mesenteric, com: combined counts; n = 3–19 mice, one-way ANOVA, counts are plotted per single lymph node.

(D) Lymph node counts after treatment with FTY720 (egress block) or integrin-blocking antibodies (homing block); n = 3–5 mice, one-way ANOVA with Tukey's multiple comparisons test.

(E) Lymphocyte subpopulations after homing block (left) and egress block (right); n = 3 mice. *p < 0.05, **p < 0.01, ****p < 0.0001. All data are represented as mean ± SEM. See also Figure S1.

Circadian rhythms are important drivers for most physiological processes as they align the body with rhythmically occurring daily changes in the environment (Dibner et al., 2010). They normally rely on an intricate interplay of cell-intrinsic clock genes driving circadian responses (Mohawk et al., 2012). Daily oscillations of lymphocyte counts in blood have been described (Arjona et al., 2012; Curtis et al., 2014; Haus and Smolensky, 1999; Labrecque and Cermakian, 2015; Scheiermann et al., 2013) and cells of the adaptive immune system such as T and B cells, as well as dendritic cells, possess the components of the molecular clock machinery (Bollinger et al., 2011; Hemmers and Rudensky, 2015; Silver et al., 2012a). In contrast to monocytes of the innate immune system (Nguyen et al., 2013), however, the functional relevance of these cell-intrinsic oscillations for lymphocytes is unclear (Hemmers and Rudensky, 2015). Stimulated by previous findings, which described periodic oscillations in innate immune cell function (Gibbs et al., 2014; Nguyen et al., 2013; Scheiermann et al., 2012) and T helper-17 (Th17) cell differentiation (Yu et al., 2013), we postulated that the migration of lymphocytes through murine LNs might be regulated in a circadian manner with direct relevance for the mounting of adaptive immune responses.

RESULTS

Lymphocyte Numbers Exhibit Circadian Oscillations in Lymph Nodes

In contrast to circulating blood lymphocyte numbers, which peak during the day in mice around *Zeitgeber* time (ZT) 5 (i.e., 5 hr after light onset) (Figure 1A), numbers for $CD4^+$ and $CD8^+$ T cells as well as B cells showed delayed oscillations (by ~8 hr) in inguinal lymph nodes (iLNs), with highest counts occurring at the beginning of the dark phase (ZT13, i.e., 1 hr after lights off) (Figure 1A). These rhythms were consistently observed for naive and central memory T cells, demonstrating a broad phenomenon also affecting T lymphocyte subpopulations (Figures S1A–S1C). Oscillations were not only observed in the rhythmic environment represented by 12 hr light:12 hr dark conditions (LD) but were sustained in constant darkness (dark:dark, DD), indicating their bona fide endogenous circadian nature (Figure 1B). Light exposure was an important entrainment factor, since rhythms were inverted when the light regime was reversed (DL) (Figure 1B). Rhythms were furthermore detected across various types of LNs (Figure 1C and Figures S1D–S1F), indicating a relevant phenomenon across the LN compartment. To investigate the

underlying mechanisms driving these oscillations, we focused on the cellular LN input and output pathways by blocking lymphocyte homing or egress, both critical determinants of LN cellularity (Lo et al., 2005). Blocking homing with anti-integrin antibodies dramatically decreased LN cellularity over 24 hr while blocking lymphocyte egress with FTY720 increased LN cellularity over the same time frame, confirming the temporally highly dynamic cellular nature of this tissue (Figures 1D and 1E). Both treatments ablated rhythmicity, indicating that lymphocyte homing and egress—but not intranodal proliferation (Figures S1G and S1H)—were the central determinants of circadian oscillatory cellularity. These data demonstrate a striking circadian oscillation in lymph node cellularity, peaking at night onset.

Lymphocyte Homing Is Dependent on Oscillations in Lymphocytes and Microenvironment

We next used adoptive transfer techniques to determine whether lymphocyte homing to the LN was occurring in a rhythmic manner. LN infiltration of lymphocyte subpopulations peaked around night onset and remained low during the day (Figure 2A). To define whether oscillations were determined by lymphocyte-intrinsic and/or microenvironmental signals, we adoptively transferred cells harvested at ZT5 (“day”) or ZT13 (“night”) into LD-entrained recipients at either ZT5 or ZT13. While “day” (cells) into “day” (recipient) transfers exhibited the lowest homing capacity and “night” into “night” transfers the highest, a mixed contribution of both lymphocyte and microenvironment timing was observed in the “day” into “night” and “night” into “day” chimeras (Figure 2B). A screen for oscillations of promigratory factors on T and B cells revealed that expression of the chemokine receptor CCR7 exhibited rhythmicity peaking at ZT13 (Figure 2C) while the adhesion molecules CXCR4, CD11a, and L-selectin showed either no oscillations or not for all lymphocyte subpopulations (Figures S2A and S2B). In addition, expression analyses of whole lymph node mRNA and extracellular protein on HEVs revealed oscillatory amounts of the chemokine CCL21, a ligand for CCR7—but not CXCL12 (not shown)—being high around night onset (Figures 2D and 2E). HEVs also exhibited rhythmic expression of ICAM-1 but not of PNAd (Figures S2C and S2D). Oscillations in lymphocyte chemokine receptors were critical for rhythmic homing because a titrated, short pretreatment of adoptively transferred cells with pertussis toxin (PTX) (Lo et al., 2005), an inhibitor of chemokine receptor signaling, ablated rhythmicity (Figure 2F). To investigate the involvement of CCR7 in this process, we analyzed total lymph node cellularity of CCR7-deficient mice, as well as the rhythmic homing capacity of isolated CCR7-deficient cells. *Ccr7*$^{-/-}$ mice exhibited no oscillations in lymph node cell counts while also exhibiting the expected lower overall numbers (Förster et al., 1999) (Figure 2G). In addition, *Ccr7*$^{-/-}$ cells failed to show rhythmic lymph node homing (Figure 2H). These data demonstrated that lymphocyte recruitment to LNs is determined by rhythms in leukocytes and the microenvironment, along with in-phase expression of the CCR7-CCL21 receptor-ligand axis.

Circadian Clocks Control Cellular Oscillations in Lymph Nodes

LNs exhibit oscillations of clock genes (Figure 3A), prompting us to investigate the role of lymphocyte clocks in their migratory behavior. We generated mice in which the core clock gene *Bmal1* (also known as *Arntl*) was deleted in T cells (*Bmal1*$^{flox/flox}$x*Cd4-cre*) or B cells (*Bmal1*$^{flox/flox}$x*Cd19-cre*) (Figure 3B and Figures S2E and S2F). Remarkably, loss of lymphocyte BMAL1 ablated the overall rhythmicity of T and B cell numbers in lymph nodes (Figure 3C and Figure S2G). In addition, rhythmic homing of *Bmal1*$^{flox/flox}$x*Cd4-cre* T cells into WT recipients was ablated (Figure 3D). In agreement with these findings, rhythmic expression of CCR7 surface protein (Figure 3E) and mRNA (Figure 3F) was absent in BMAL1-deficient CD4$^+$ T cells, indicating the regulation of the molecule at the transcriptional level by the circadian clock. Together, these data provide evidence for a functional role of cell-autonomous clocks in lymphocyte migration.

Lymphatic Egress from Lymph Nodes Is under Circadian Control

Because our data indicated that, in addition to a rhythmic homing component, lymphocyte egress might counterbalance LN oscillations (Figures 1D and 1E), we quantified lymphocyte numbers in lymph fluid by cannulating efferent lymphatic vessels. Prominent rhythms in cellular counts were detected, peaking at ZT9 and exhibiting a low at ZT21 (Figure 4A). These oscillations were observed for different lymphocyte populations (Figure 4A and Figures S2H and S2I) and were bona fide circadian in nature as they persisted in constant darkness (Figure 4B). Rhythms were not due to higher lymph volume or flow rates at different times of the day (Figure S2J). To verify whether oscillations in lymph cellularity were truly attributable to rhythmic egress and not secondary to rhythmic input into LNs (Figure 2A), we transferred lymphocytes at different times of the day, blocked subsequent LN entry and quantified their transit through the LN into lymph over time (Mandl et al., 2012). A higher LN retention capacity of cells injected at ZT13 was observed compared to ZT5 and a less rapid accumulation of cells in lymph (Figures 4C and 4D and Figure S3), demonstrating lymphocyte egress to be highly rhythmic. This effect resulted in longer LN half-lives of cells injected at ZT13 (CD4: 12 hr, CD8: 12 hr, B cells: 16 hr) compared to ZT5 (CD4: 9 hr, CD8: 9 hr, B cells: 13.5 hr) (Figures 4C and 4D and Figure S3). T- and B cell-specific BMAL1-deletion ablated oscillations in lymph, indicating the importance of cell-autonomous clocks also for lymphocyte egress (Figure 4E and data not shown). Of importance, adoptively transferred BMAL1-deficient CD4$^+$ T cells exhibited no time-of-day variations in their LN half-life (Figure 4F), demonstrating the relevance of T cell clocks in their rhythmic trafficking behavior.

Using a mathematical approach, we assessed whether oscillatory LN counts could be modeled with only either homing or egress to be rhythmic or whether both components needed to oscillate. Although oscillations were also observed when only one component was rhythmic, the best fit was achieved when both homing and egress were assumed to oscillate, thus supporting our experimental data (Figure 4G and Figure S4). In summary, lymphocyte clocks and the time-of-day entry of cells into LNs have functional consequences for LN transit and egress into lymph.

Rhythmic Lymphocyte Egress Depends on Oscillatory *S1pr1* Expression

S1P-receptors are critical in regulating lymph node egress (Cyster and Schwab, 2012). We therefore investigated whether

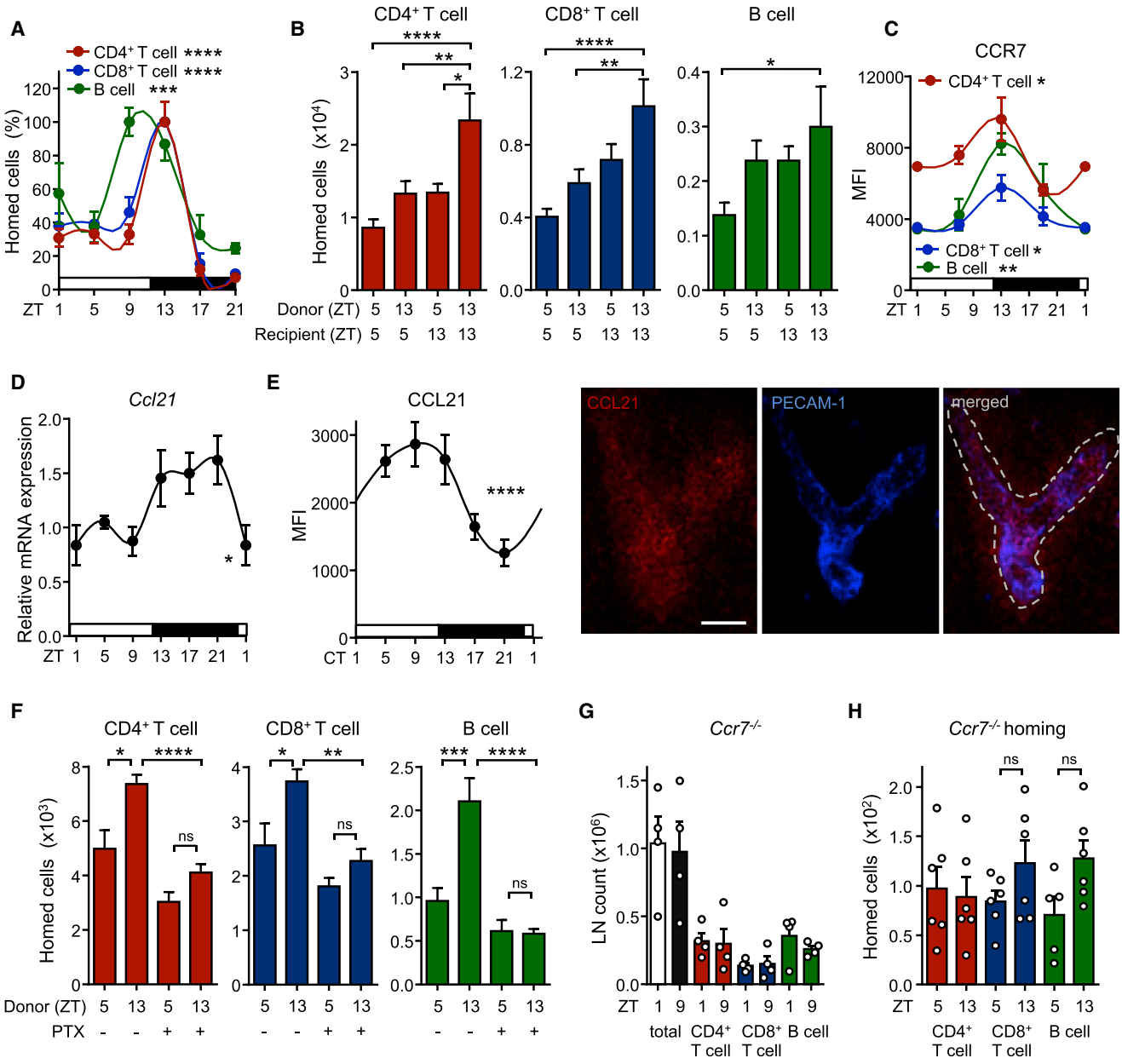

Figure 2. Rhythmic Lymphocyte Homing Is Dependent on Oscillations in Both Lymphocytes and Microenvironment

(A) Lymph node homing of lymphocyte populations over the course of the day, normalized to peak times; n = 3–17 mice, one-way ANOVA.

(B) Adoptive transfer of lymphocyte populations using donor and recipient mice kept at ZT5 or ZT13; n = 6–17 mice, one-way ANOVA with Tukey's multiple comparisons test.

(C) Oscillations of CCR7 surface expression on lymphocyte subpopulations in LN; n = 3–5 mice, one-way ANOVA.

(D) Q-PCR analysis of LN *Ccl21* amounts over 24 hr; n = 3–5 mice, one-way ANOVA.

(E) Quantification and images of expression of CCL21 on HEV over 24 hr in constant darkness (CT, circadian time: the corresponding light and dark phase are indicated); n = 3–18 mice, one-way ANOVA. Scale bar represents 50 μm.

(F) LN homing of lymphocytes harvested at ZT5 or ZT13 and treated with or without pertussis toxin (PTX); n = 5–11 mice, one-way ANOVA with Tukey's multiple comparisons test.

(G) Lack of oscillations in LN cellularity of *Ccr7*$^{-/-}$ mice; n = 4 mice, unpaired Student's t test.

(H) Lack of rhythmic LN homing of *Ccr7*$^{-/-}$ cells into WT hosts; n = 5–6 mice, unpaired Student's t test. *p < 0.05, **p < 0.01, ***p < 0.001, ****p < 0.0001. All data are represented as mean ± SEM. See also Figure S2.

expression of S1P-receptor family members exhibited oscillations using quantitative PCR (Q-PCR). All S1P receptors exhibited robust diurnal oscillations peaking between ZT1 and ZT9 (Figure 5A and Figure S5A), which coincided with high lymphocyte egress. In addition, FTY720, as well as the S1P1-specific functional antagonist SEW2871 strongly down-modulated lymphatic

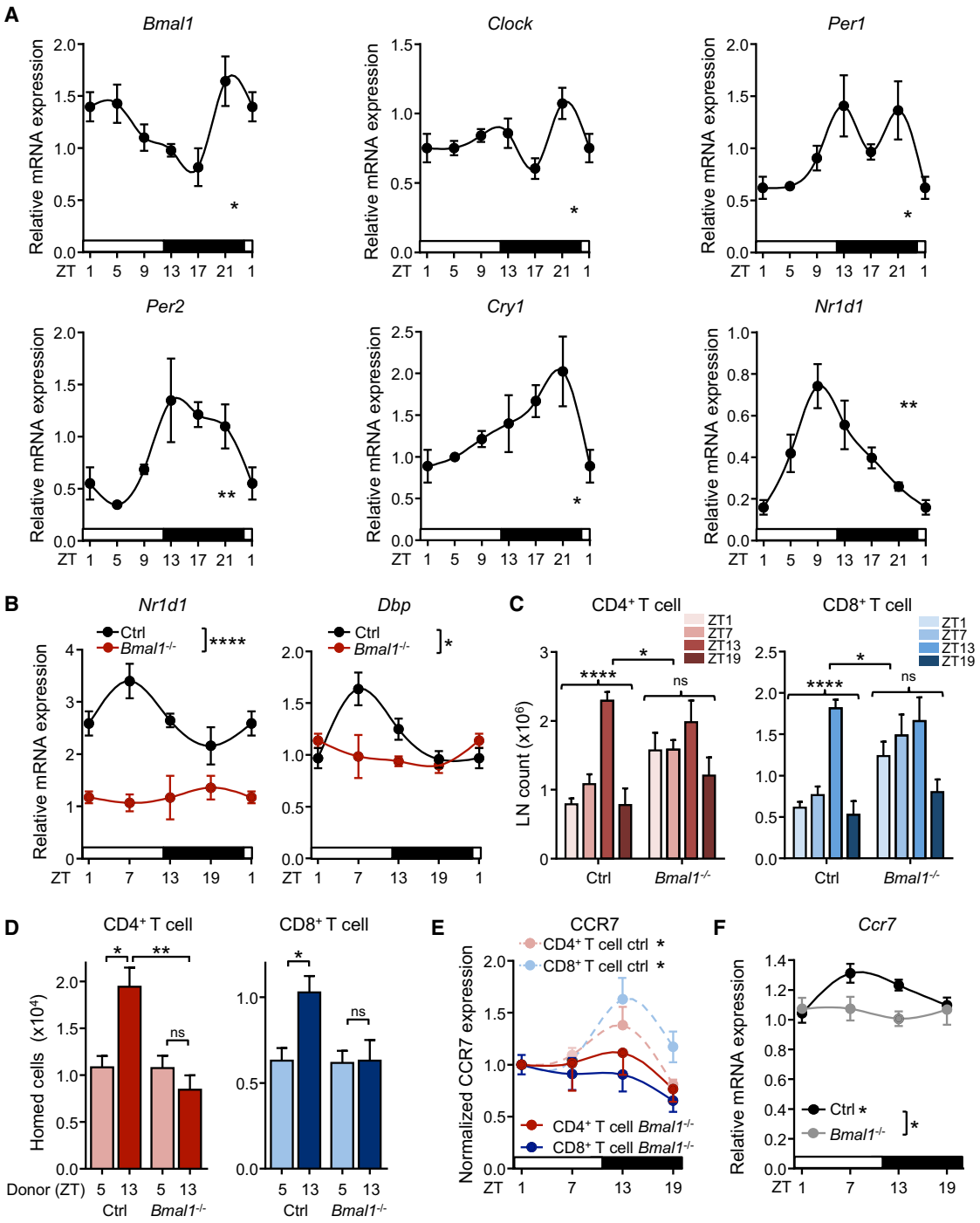

Figure 3. Oscillations of Circadian Clock Genes in Lymph Nodes Control Cellularity

(A) Q-PCR analysis of circadian clock genes in LN over 24 hr; n = 3–5 mice, one-way ANOVA.

(B) Circadian clock gene mRNA profiles in sorted CD4$^+$ T cells from *Bmal1*$^{flox/flox}$x*Cd4-cre* and control animals; n = 3–10 mice, two-way ANOVA.

(C) Lymph node CD4 and CD8 T cell counts in control and T cell specific *Bmal1*$^{-/-}$ mice, n = 3–9 mice, one-way and two-way ANOVA.

(D) LN homing of lymphocytes harvested from control or T cell-specific *Bmal1*$^{-/-}$ mice at ZT5 or ZT13 into WT hosts; n = 10–34 mice, one-way ANOVA with Tukey's multiple comparisons test.

(E) CCR7 surface expression on T lymphocyte subpopulations in LN of control and T cell-specific *Bmal1*$^{-/-}$ mice; n = 3–5 mice, one-way ANOVA.

(F) Q-PCR analysis of CD4$^+$ T cell *Ccr7* over 24 hr in control and T cell-specific *Bmal1*$^{-/-}$ mice; n = 4–8 mice, one-way and two-way ANOVA. *p < 0.05, **p < 0.01, ****p < 0.0001. All data are represented as mean ± SEM. See also Figure S2.

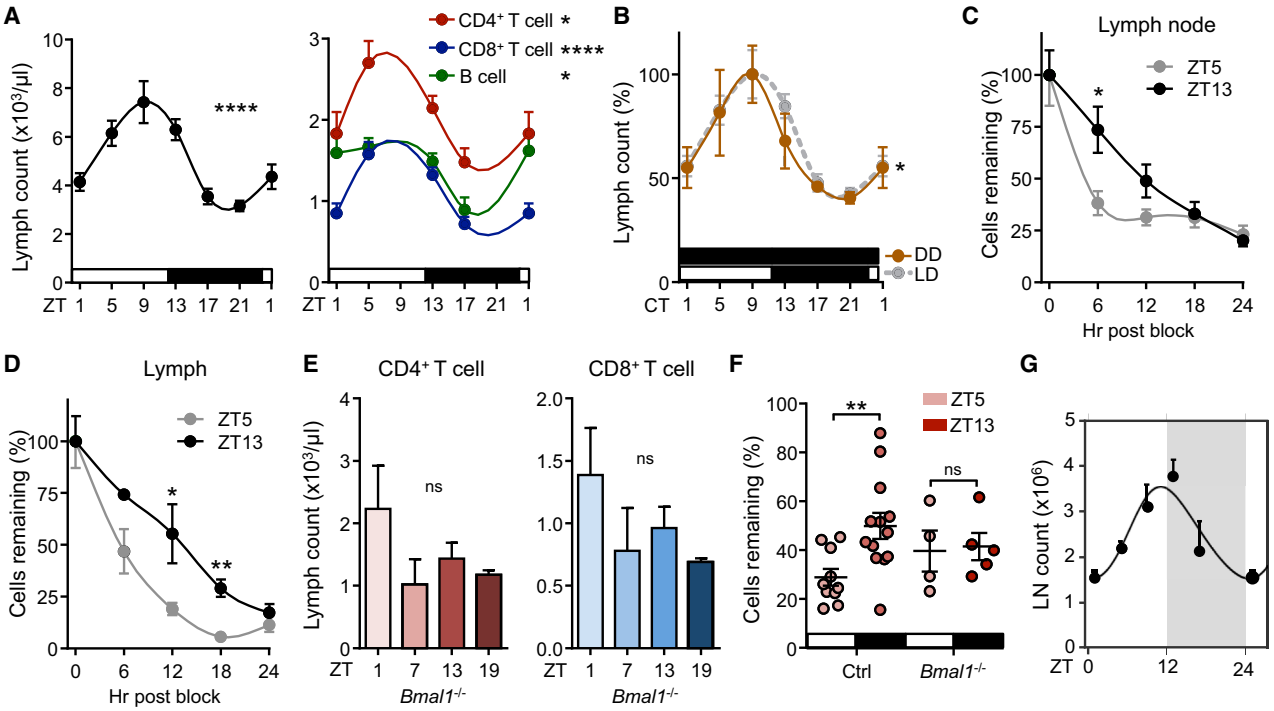

Figure 4. Circadian Oscillations in Lymphocyte Egress from LNs

(A) Oscillations of total leukocyte (left panel) and lymphocyte (right panel) counts in efferent lymph over 24 hr; n = 6–33 mice, one-way ANOVA.

(B) Lymph leukocyte count oscillations under light-dark (LD) and dark-dark (DD) conditions; n = 3–37 mice, one-way ANOVA.

(C and D) Remaining cellular numbers (in %) in lymph node (C) and lymph (D) over 24 hr after block of leukocyte homing. Lymph node: n = 3–10 mice; lymph: n = 3–6 mice, unpaired Student's t test.

(E) Lymph CD4$^+$ and CD8$^+$ T cell counts in T cell-specific *Bmal1*$^{-/-}$ mice; n = 3–8 mice, one-way ANOVA.

(F) Remaining cells (in %) in lymph nodes of adoptively transferred control and BMAL1-deficient CD4$^+$ T cells 12 hr after transfer; n = 4–13, unpaired Student's t test.

(G) Mathematical model of leukocyte homing and egress. The model is expressed as a line based on the indicated data points. *$p < 0.05$, **$p < 0.01$, ****$p < 0.0001$. All data are represented as mean ± SEM. See also Figures S2–S4.

egress in a time- and concentration-dependent manner (Figures 5B and 5C and Figure S5B). The observation that FTY720-treated animals exhibited reduced but still rhythmic lymph cellularity indicated a daytime-sensitive role for S1P1 in mediating lymphocyte exit. Rhythmic expression of *S1pr1* was ablated in BMAL1-deficient CD4$^+$ T cells, pointing toward a regulation of the gene by the circadian clock (Figure 5D). To investigate this in more detail, we performed an in vitro assay, in which the promoter region of *S1pr1* was cloned in front of the luciferase (*luc*) reporter gene. Luciferase activity in HEK293 cells transfected with the *S1pr1-luc* reporter was decreased after co-transfection of increasing amounts of *Bmal1* and *Clock* expression plasmids (Figure 5E). This demonstrated that expression of *S1pr1* is regulated by BMAL1 and CLOCK.

To confirm the role of S1P1 in the time-of-day-dependent egress genetically, we generated T cell-specific mice that were heterozygous for *S1pr1* in order not to completely block lymphocyte egress (Matloubian et al., 2004) but to titrate S1P1 amounts, as loss of one allele had been demonstrated to result in haploinsufficiency (Lo et al., 2005). *S1pr1*$^{+/flox}$*xCd4-cre* mice exhibited no more oscillations in LN counts and altered lymph rhythmicity, demonstrating the importance of S1P1 in the proper timing of lymphocyte egress (Figures 5F and 5G and Figure S5C). Importantly, no diurnal oscillations were observed in amounts of S1P in efferent lymph (Figure 5H) or in S1P synthesizing or degrading enzymes in lymph node (Figure S5D), suggesting that oscillatory expression of the receptor (S1P1) and not its ligand (S1P) was the driver for rhythmic lymphocyte egress. Together, these data demonstrate a critical role for S1P1 in mediating circadian lymphocyte egress from lymph nodes into efferent lymph.

Relevance of Circadian Oscillations in Lymph Node Cellularity

We hypothesized that oscillatory lymphocyte counts in LNs might have functional consequences in a potential time-of-day dependence of adaptive immune responses. We therefore tested whether the activation status of lymphocytes in LNs varied over the course of the day. More activated T cells were present in LNs at night onset as assessed by CD69 staining, coinciding with higher overall lymphocyte counts at this time (Figure 6A). Because dendritic cells (DCs) are key antigen-presenting cells critical in the activation of lymphocytes and the generation of adaptive immune responses (Girard et al., 2012), we

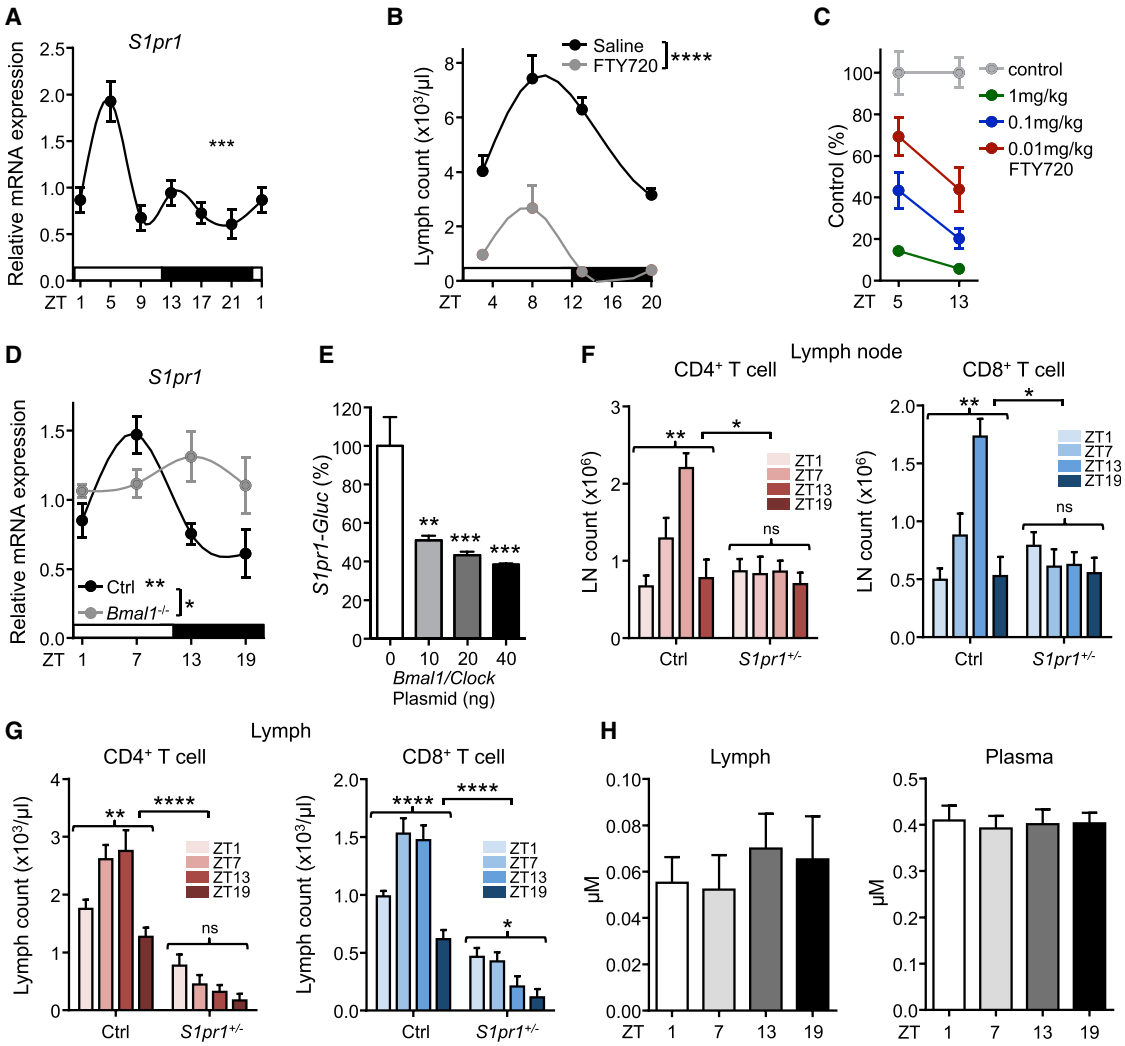

Figure 5. Rhythmic Lymphocyte Egress Depends on Oscillatory S1pr1 Expression

(A) Q-PCR analysis of LN *S1pr1* over 24h. n = 3–5 mice, one-way ANOVA.

(B) Lymph counts after blockade of S1P-receptor function using FTY720 at the indicated times; n = 3–33 mice, two-way ANOVA.

(C) FTY720 titration and respective lymph counts at two time points. n = 3–5 mice.

(D) Q-PCR analysis of CD4$^+$ T cell *S1pr1* over 24 hr in control and T cell-specific *Bmal1*$^{-/-}$ mice; n = 4–9 mice, one-way and two-way ANOVA.

(E) Normalized activity (in %) of Gaussia Luciferase driven by murine *S1pr1* promoter (*S1pr1*-GLuc) after co-transfection with various doses of *Clock* and *Bmal1* plasmids in HEK293 cells (n = 6). Data shown are pooled from two independent experiments, one-way ANOVA with Tukey's multiple comparisons test.

(F) LN CD4$^+$ and CD8$^+$ T cell counts in control and T cell-specific *S1pr1* heterozygous mice; n = 3–6 mice, one-way and two-way ANOVA.

(G) Lymph CD4$^+$ and CD8$^+$ T cell counts in control and T cell-specific *S1pr1* heterozygous mice; n = 3–12 mice, one-way and two-way ANOVA.

(H) Mass spectrometric analysis of sphingosine-1-phosphate (S1P) in lymph and blood plasma; n = 9–11 mice. *p < 0.05, **p < 0.01, ***p < 0.001, ****p < 0.0001. All data are represented as mean ± SEM. See also Figure S5.

next investigated whether these cells also exhibited oscillatory LN counts. Migratory DC cellularity showed strong oscillations peaking in phase with lymphocytes (Figure 6B and Figure S6A). These data point to the existence of a concerted circadian migration pattern of antigen-bearing (DCs) and antigen-recognizing (T cells) cells in LNs.

Recent evidence indicates that the immune system can respond to challenges in a rhythmic fashion (Fortier et al., 2011; Gibbs et al., 2014; Nguyen et al., 2013; Scheiermann et al., 2012; Silver et al., 2012b). We therefore investigated the pathophysiological significance of circadian oscillatory LN counts in the autoimmunity model of EAE. Mice immunized during the late light phase (ZT8, when cell counts are high in LNs, Figures 1A and 1C) showed a dramatically accelerated disease progression 2 weeks later, with higher clinical scores compared to late night-immunized animals (ZT20, when LN counts trough) (Figure 6C). Differences in disease scores were associated with higher immune cell infiltration and demyelination in the spinal cord at the peak of the disease (Figures 6D and 6E). We detected elevated interleukin-2 (*Il2*) mRNA amounts (Figure 6F) and a higher number of IL-17 producing as well as very-late antigen (VLA)-4 integrin positive CD4$^+$

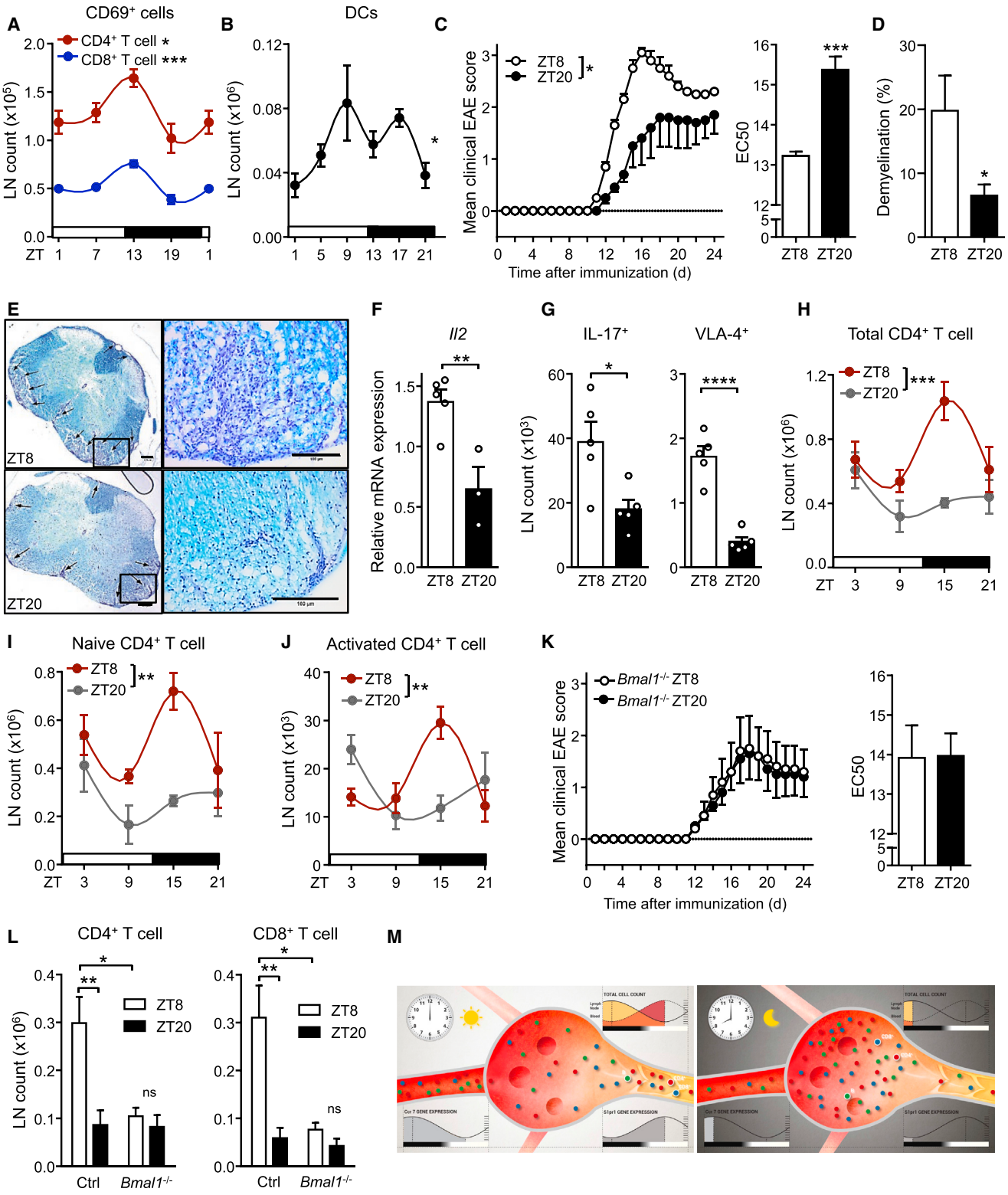

Figure 6. T Cell Clock Function Regulates Disease Severity in EAE

(A) Oscillations of CD69$^+$ T cell numbers in lymph node; n = 3–5 mice, one-way ANOVA.

(B) Oscillations of migratory dendritic cells (DCs) in lymph node; n = 6–12 mice, one-way ANOVA.

(C) EAE disease scores of mice immunized at ZT8 or ZT20. Disease score EC_{50} comparisons show accelerated symptom progression in ZT8-immunized mice; n = 5 mice, two-way ANOVA (left panel) and unpaired Student's t test (right panel).

(legend continued on next page)

T cells in LNs of ZT8-immunized mice, subtypes that have been shown to be critical for the induction of EAE (Kawakami et al., 2012) (Figure 6G). This indicated that circadian regulation of immunization occurred at a very early phase of the process when T cells are activated in draining lymph nodes (Figure S6B). Two days after induction of EAE, an increase of both naive and activated $CD4^+$ and $CD8^+$ T cells was detected in draining lymph nodes of ZT8-immunized animals, while in ZT20-immunized animals T cell numbers remained relatively low (Figures 6H–6J and Figure S6C). Thus, oscillations in the numbers of $CD4^+$ T cells in lymph nodes during initial encounter with antigen appear to be pivotal for the severity of EAE. To investigate whether T cell autonomous clocks regulate this response, we genetically deleted T cell circadian clock function. Although in control animals disease development depended on the time of immunization, in T cell specific *Bmal1*$^{-/-}$ mice it did not (Figure 6K). Two days after immunization, total and T cell counts in draining lymph nodes were different at ZT15 between day- and night-immunized control, but not in T cell specific *Bmal1*$^{-/-}$ mice (Figure 6L and Figure S6D). Hence, T cell clocks determine time-of-day function and, after challenge, development of autoimmune sequelae. We finally investigated whether adaptive immune responses to pathogens exhibited similar circadian rhythmicity. Mice were infected with the gastric bacterial pathogen *Helicobacter pylori* at three different time points during the day, and lymph node counts were quantified 3 weeks later. Also in this chronic infection model, LN counts showed strong circadian responsiveness to the initial infection with highest numbers present at ZT7, analogous to the EAE immunization experiments (Figure S6E). In addition, acute viral infection with influenza A virus led to stronger pulmonary infiltration of $CD8^+IFN\text{-}\gamma^+$ T cells when animals were infected at ZT8 compared to ZT20, 8 days post infection (Figure S6F). Together, these data strongly indicate that immunization reactions and the adaptive immune responses to various pathogens follow a circadian rhythm (Figure 6M and Movie S1).

DISCUSSION

We have described here the mechanisms that govern a circadian rhythmicity in the capacity of lymphocytes to enter and exit lymph nodes, which depend on cell-autonomous, clock-gene-controlled expression of promigratory factors. Lymphocytes entered LNs most prominently at the onset of the night phase and egressed from the tissue during the day. This resulted in oscillatory cell counts in lymph nodes and lymph and time-of-day differences in the adaptive immune response weeks after immunization. In addition, DCs were found to be present in LN in highest numbers around night onset, peaking in phase with the lymphocyte populations. Our data reveal that T cell-autonomous circadian oscillations are critical in regulating adaptive immunity.

It is surprising to note that lymph nodes exhibit circadian differences in their cellularity, given that they represent such a central tissue of the immune system and, accordingly, have thus been intensely studied. Since we observed oscillations in all investigated lymph nodes, the phenomenon appears to be broad and robust and not restricted to specific body locations. It is noteworthy that other lymphoid organs such as the thymus (data not shown) and the bone marrow do not exhibit overt circadian oscillations in absolute numbers. At least the latter, however, still displays circadian activity in cellular trafficking as hematopoietic stem and progenitor cells (HSPCs) are mobilized into blood (Lucas et al., 2008; Méndez-Ferrer et al., 2008) and recruited back into the bone marrow (Scheiermann et al., 2012) at different times. The fraction of mobilized and homed cells might be small compared with the overall numbers, though, which might explain why overt oscillations of total cells in the BM are not observed. In contrast to the BM, lymph node total cellularity is highly dynamic over 24 hr, as seen when homing or egress is blocked. Still, homing of leukocytes to lymph nodes and bone marrow occurs predominantly at night, while egress (or mobilization in the case of the bone marrow) occurs predominantly during the day. Thus, rhythmic egress of lymphocytes via efferent lymph is a major mechanism underlying the oscillatory leukocyte numbers in blood. Whether other egress routes for lymphocytes, from the thymus or the spleen, occur in a circadian manner is currently unclear.

Our data point to a critical role of cell-intrinsic clock-dependent mechanisms in the regulation of T and B lymphocyte trafficking. While global BMAL1 deficiency results in a diverse array of phenotypes (Bunger et al., 2000), such as altered B cell numbers (Sun et al., 2006), few studies have focused on cell-type specific deletion of BMAL1 in the immune system. Lineage-specific ablation of BMAL1 in myeloid cells results in a pro-inflammatory state (Nguyen et al., 2013), yet a similar approach targeting lymphocytes yielded no obvious phenotype (Hemmers and Rudensky, 2015). The latter finding might be due to mice with clock-deficient lymphocytes exhibiting phenotypes only at specific times, so that only when tested over multiple time points across the day can alterations be detected.

(D) Quantification of demyelination in lumbar spinal cord sections; n = 5 mice, unpaired Student's t test.
(E) Luxol Fast Blue staining of lumbar spinal cord sections of mice immunized at ZT8 (top) or ZT20 (bottom) at the peak of the disease showing demyelinated areas (arrows), scale bar represents 200 μm (left images), 100 μm (right images).
(F) LN IL-2 mRNA after EAE induction; n = 3–5 mice, unpaired Student's t test.
(G) LN counts of $IL\text{-}17^+$ and $VLA\text{-}4^+$ $CD4^+$ T cells after EAE induction; n = 5 mice, unpaired Student's t test.
(H–J) Diurnal profiles of inguinal lymph node counts of total $CD4^+$ T cells (H), naive $CD4^+$ T cells (I), and activated $CD4^+$ T cells (J) on day 2 after EAE induction; n = 4 mice, two-way ANOVA with Bonferroni's post hoc test.
(K) EAE disease scores and EC_{50} values in T cell-specific *Bmal1*$^{-/-}$ mice immunized at ZT8 or ZT20; n = 5 mice.
(L) Inguinal lymph node counts of $CD4^+$ T cells, and $CD8^+$ T cells in T cell-specific *Bmal1*$^{-/-}$ mice at ZT15 on day 2 after EAE induction; n = 4–5 mice, unpaired Student's t test.
(M) Schematic diagram of circadian lymphocyte migration through lymph nodes. At night onset, increased homing due to higher CCR7 amounts leads to enhanced lymphocyte counts in the lymph node. During the day, higher *S1pr1* expression induces the egression of lymphocytes into efferent lymph. *$p < 0.05$, **$p < 0.01$, ***$p < 0.001$, ****$p < 0.0001$. All data are represented as mean ± SEM. See also Figure S6 and Movie S1.

Our data showing that lack of BMAL1 in T cells ablated oscillations in EAE disease scores indicates an important role for T cell clocks in the adaptive immune response. This is in line with a previous observation that T cells harvested from *Clock* mutant mice exhibited altered proliferation responses at specific times (Fortier et al., 2011).

We demonstrated the critical regulators of lymphocyte trafficking, *Ccr7* and *S1pr1*, to be under circadian control. *Ccr7* and *S1pr1* oscillations showed opposite phases, being high in the evening for the former and high during the day for the latter. This agrees with the additional role of CCR7 as a retention factor for T cells in lymph nodes that can antagonize S1P1 function (Pham et al., 2008). In addition, more T cells expressed the activation marker CD69 at night onset, a negative regulator of S1P1 (Shiow et al., 2006). These inverted oscillations of retention and egress factors appeared to be responsible for keeping lymphocytes retained in the node at night and promoting daytime egress. In addition to these lymphocyte intrinsic signals, the microenvironmental fluctuation of CCL21 indicated an additional rhythmic component that was non cell-autonomous. Whether direct autonomic innervation governs these oscillations—as has been shown for the bone marrow and skeletal muscle (Méndez-Ferrer et al., 2008; Scheiermann et al., 2012)—and/or humoral factors as has been shown for the lung (Gibbs et al., 2014), is outside the scope of this manuscript and should be investigated in the future.

Lymph nodes act as the body's immunological sieve, capturing lymph-borne antigens and antigen-presenting cells (APCs) and bringing these components in close contact with lymphocytes. Our data show that not only T cells migrate to the lymph node in a circadian manner but that also dendritic cells, the major APCs, are present more prominently around night onset, peaking at the same time as lymphocytes. Both cell types need to interact to produce a functional adaptive immune response (Gasteiger et al., 2016). It therefore appears likely that having them present at the same time in the confined environment of the lymph node enhances the likelihood of antigen encounter by the very few specific T cell clones, as opposed to cells entering and exiting at random times. This process of more effective cellular interactions appears to be further helped by the fact that during the night fewer cells exit the tissue than during the day, thus giving APC-T cell pairs more time to interact functionally. Whether also antigen encounter with APCs at peripheral surfaces is occurring in a rhythmic manner, which could ultimately be driving a circadian migratory DC process, should be the subject of future investigations.

Compared to the immediate response of the innate immune system, which is under circadian control (Gibbs et al., 2014; Keller et al., 2009; Nguyen et al., 2013; Scheiermann et al., 2012), it is remarkable that also the adaptive immune system appears to be temporally regulated, because these responses take much longer to be mounted. How can the time-of-day dependent differences encountered during the initial stimulus be preserved to exhibit circadian gating of immune responses weeks later? It appears that the initial hours in the generation of the adaptive immune response and the number of cells present in the lymph node are critical in regulating the strength of the response (Moon et al., 2007), which cannot be compensated for by the next circadian cycle.

In steady state, critical factors of the immune system oscillate in mice and humans with opposite phases according to their inverted rest-activity times (Arjona et al., 2012; Curtis et al., 2014; Labrecque and Cermakian, 2015; Scheiermann et al., 2013). Circulating leukocyte counts are high during the respective resting phases, which occur during the day in mice and at night in humans. In addition, also under stimulated conditions timing matters, as administration of granulocyte colony-stimulating factor (G-CSF) to patients in order to mobilize hematopoietic stem cells from bone marrow into blood yields higher numbers at different times than in mice (Lucas et al., 2008). These data suggest that also adaptive immune responses in humans could be under circadian control. Since in our EAE model, immunization close to the onset of the activity phase produced a higher immune response in mice, in humans the early morning hours should produce a higher adaptive immune reactivity. Indeed, this appears to be the case as recent studies have unveiled that administration of hepatitis A (Phillips et al., 2008) and flu vaccines (Long et al., 2016) in the morning yielded highest antibody titers compared to other times. Together, our data provide mechanistic insights for a time-of-day difference in lymphocyte trafficking and adaptive immune responses, thus warranting further investigations into time-of-day optimization of immune therapies and vaccination programs.

EXPERIMENTAL PROCEDURES

Animals

Cd4cre, *Lckcre*, *Cd19cre*, *Bmal1*$^{flox/flox}$, and *S1pr1*$^{flox/flox}$ mice were obtained from Jackson Laboratories and crossbred to target T cells and B cells, respectively. *Ccr7*$^{-/-}$ mice were a gift from Reinhold Förster. 7- to 8-week-old wild-type C57BL/6 mice were purchased from Charles River and Janvier. Mice were housed under a 12 hr:12 hr light-dark cycle with food and water ad libitum. To induce changes in light regime, we placed mice in a light cycler (Park Bioservices) with a 12 hr-inverted light cycle for a minimum of 2 weeks to completely establish an inverse light cycle or kept in constant darkness. All animal experimental procedures were carried out in accordance with the German Law of Animal Welfare and approved by the Regierung of Oberbayern or the ethics committee of the Schleswig-Holstein State Ministry of Energy, Agriculture, Environment and Rural Areas.

Flow Cytometry

Blood was collected into EDTA-coated capillary tubes (Microvete 300). Counts were obtained using an IDEXX ProCyte DX cell counter or a Hemavet Hematology Analyzer 950FS (Drew Scientific). Erythrocytes were lysed by incubation in 0.8% NH_4Cl. Lymph was collected as described below. Spleens, lymph nodes, or thymi were harvested from animals and processed through a cell strainer (40–70 μM pore size) and resuspended in PBS. For quantification of dendritic cells, lymph nodes were first chopped into small pieces and incubated in collagenase IV (1 mg/ml, C5138, Sigma) and DNase I (0.2 mg/ml, Roche) for 30 min at 37°C with gentle agitation. Following digestion, cells were passed through a 40 μm strainer and resuspended in PBS supplemented with 2% fetal bovine serum (GIBCO). A 20 min blocking step using anti-CD16/32 antibody (2.4G2; BD Biosciences) was performed on ice prior to fluorescent staining. Single-cell suspensions were stained with fluorescence-conjugated antibodies and analyzed by flow cytometry using a Gallios Flow Cytometer (Beckman Coulter) or a FACSCanto II flow cytometer (BD Biosciences). Prior to staining of intracellular cytokines, cells were restimulated for 5 hr with PMA and ionomycine (cell stimulation cocktail with protein transport inhibitors, eBioscience). Data were analyzed with FlowJo software (Tree Star).

Adoptive Transfer Studies

Lymphocytes from spleen and peripheral lymph nodes (ratio 80:20) were labeled with 1.5 μM of carboxyfluorescein succinimidyl ester (CFSE,

Thermo Fisher Scientific) or 2.5 μM CellTracker Red CMTPX (Thermo Fisher Scientific) in PBS containing 0.2% BSA and 2 mM EDTA for 20 min at 37°C and washed 4 times. 20 × 10^6 cells were then injected i.v. into recipient mice. In some experiments, lymph node entry was blocked two and 12 hr later by intraperitoneal (i.p.) administration of 100 μg anti-α_L (CD11a, clone M17/4; BioXCell) and anti-α_4 (CD49d, clone PS/2; BioXCell) integrin antibodies in PBS. In some experiments, cells were pre-incubated with a 200 ng/ml pertussis toxin (PTX) pulse of 10 min at 37°C and washed 4 times before injection together with control-treated cells (Lo et al., 2005). The subsets of adoptively transferred cells in the recipient mice were analyzed via flow cytometry. Dyes were switched to avoid dye-specific effects.

S1pr1 Promoter Luciferase Reporter Assay

The *S1pr1*-Gaussia Luciferase (*S1pr1*-GLuc) GLuc-ON promoter clone containing a ~1 kb fragment upstream of the transcription start site and a ~0.3 kb fragment of the exon 1 of murine *S1pr1* in pEZX-PG04 vector (also containing a constitutively expressed secreted alkaline phosphatase (SEAP) secondary reporter as an internal control) was obtained from GeneCopoeia. HEK293AAV cells (Cellbiolabs) were plated onto 96-well plates and maintained in DMEM with 2 mM stable glutamine supplemented with 10% fetal bovine serum (FBS) and 10,000 U penicillin/streptomycin at 37°C with 5% CO2. Upon 80%–90% confluence, cells were transfected with the following expression plasmids: 20 ng *S1pr1-luc* with various combinations of the following clock gene constructs: *HA-Clock*, *HA-Bmal1*, and *pcDNA3.1* (mock transfection) as indicated per well using Lipofectamine 3000 transfection reagent (Thermo Fisher Scientific) according to the manufacturer's protocol. Medium was changed once on the next day and was collected for measurement 48 hr after transfection. The secreted GLuc and SEAP activities were measured with the Secrete-Pair Dual Luminescence Assay Kit (GeneCopoeia) according to the manufacturer's protocol using the Berthold TriStar LB 941 plate reader (Berthold Technologies). Normalized promoter activity was calculated as the ratio of GLuc to SEAP activities.

Lymph Cannulation

40 min prior to cannulation, 200 μl olive oil was administered intragastrally to identify mesenteric lymph vessels that are located just upstream of the thoracic duct. Mice were anesthetized (100 mg/kg ketamine, 20 mg/kg xylazine, 1% acepromazin i.p.), vessels were cannulated and lymph was drawn via a fine bore polythene tubing (Smiths Medical) that had previously been flushed with PBS containing EDTA. In some experiments, mice were injected i.p. with 1 mg/kg (or less) of FTY720 or 10 mg/kg of SEW2871 1 or 2 hours, respectively, before cannulation. Cell numbers were determined using an IDEXX ProCyte DX cell counter.

Immunofluorescence Microscopy and Quantitative Imaging Analysis

Harvested lymph nodes were embedded in OCT (TissueTec), frozen and sectioned with a thickness of 10 μm on a cryostat (Leica). Sections were fixed in methanol or left unfixed, incubated with fluorescently coupled antibodies and imaged on an Axio Examiner.D1 microscope (Zeiss) equipped with LEDs of 405 nm, 488 nm, 561 nm, and 642 nm excitation wavelengths or equipped with a 4-color laser stack and a confocal spinning-disk head (Intelligent Imaging Innovations). For investigations of protein expression in HEVs, all quantifications were performed using mask analysis (Zeiss software) based on PECAM-1 expression and quantifying expression of other fluorescent channels within the mask containing PECAM+-pixels delineating HEV vascular structures as previously detailed (Scheiermann et al., 2012).

EAE Induction

For EAE induction the MOG35-55-CFA Emulsion PTX Kit (EK-2110, Hooke Labs) was used according to the manufacturer's protocol. Mice were anesthetized (100 mg/kg ketamine and 10 mg/kg xylazine i.p.) and bilaterally s.c. injected with 200 μg myelin oligodendrocyte glycoprotein (MOG) 35–55 in 200 μL Complete Freund's Adjuvant (CFA) at the indicated time points, followed by two i.p. injections of 200 ng pertussis toxin (PTX) in phosphate buffered saline (PBS), immediately after immunization and 24 hr later. From day 8 on, paralysis was assessed using the clinical scoring system: 0, no obvious signs of disease; 0.5, distal paralysis of the tail; 1, complete tail paralysis; 1.5, mild paresis of one or both hind legs; 2, severe paresis of both hind legs; 2.5, complete paralysis of one hind leg; 3, complete paralysis of both hind legs; 3.5, complete paralysis of hind legs and paresis of one front leg. Animals with scores of 2 and up were provided access to food and water on the bottom of the cage.

T and B Cell Isolation

$CD4^+$ T cells for Q-PCR analysis were purified from lymph nodes of C57BL/6 WT, × *S1pr1*$^{+/flox}$x*Cd4-cre*, *Bmal1*$^{flox/flox}$x*Cd4-cre* or littermate control mice using the EasySep Mouse $CD4^+$ T cell enrichment kit (StemCell Technologies). Purity was confirmed via flow cytometry and was generally > 96%. $B220^+$ B cells for western blot analysis were purified from spleens of *Bmal1*$^{flox/flox}$x*Cd19-cre* or littermate control mice using the EasySep Mouse B cell enrichment kit (StemCell Technologies). The Pan T Cell Isolation Kit (Miltenyi Biotec) was used to purify total T cells from mouse splenocytes. Splenocytes were labeled with a mixture of biotin-conjugated monoclonal antibodies directed against cells other than T cells and followed by conjugate binding with anti-biotin microbeads. Magnetically labeled non-T cells were depleted with autoMACS (Miltenyi Biotec) and the negative fraction was collected, yielding an average 90% purity of ($CD3^+$) T cells.

Antibodies, Western Blotting, Mass Spectrometry Analyses, Quantitative Real-Time PCR, Histology, T Cell Proliferation Analyses, *Helicobacter Pylori* Infection and Influenza A Virus Infection

See Supplemental Experimental Procedures.

Statistical Analyses

All data are represented as mean ± SEM. Comparisons between two samples were performed using the paired and unpaired Student's t tests or Mann-Whitney test. One-way ANOVA analyses followed by Tukey's multiple comparison test, two-way ANOVA analyses followed by Bonferroni's post hoc test were used for multiple group comparisons. Statistical analyses were performed with GraphPad Prism 6 software. Statistical significance was assessed as $^*p < 0.05$, $^{**}p < 0.01$, $^{***}p < 0.001$, and $^{****}p < 0.0001$.

SUPPLEMENTAL INFORMATION

Supplemental Information includes six figures and Supplemental Experimental Procedures and can be found with this article online at http://dx.doi.org/10.1016/j.immuni.2016.12.011.

AUTHOR CONTRIBUTIONS

D.D. and O.M. designed and performed experiments, analyzed results, and wrote the manuscript; L.I., U.H., R.H., W.H., A.H.T., A.L., M.E., C.-S.C., K.K., A.d.J., S.M.H., N.K., O.U., L.Y., and L.E.S. performed experiments and provided valuable inputs on the manuscript; C. Schmal and H.H. performed modeling analyses; B.K. provided access to mass spectrometers; W.S. and H.O. designed and supervised experiments, discussed data, and wrote the manuscript; C. Scheiermann conceived and supervised the study, designed and performed experiments, discussed data, and wrote the manuscript.

ACKNOWLEDGMENTS

We thank Reinhold Förster and Leandro Moschovakis for providing *Ccr7*$^{-/-}$ mice, Steffen Massberg, Markus Sperandio, and Martha Merrow for critical comments on the manuscript and Victor Lavilla for designing the video. This work was supported by the German Research Foundation (DFG) (Emmy-Noether grant (SCHE 1645/2-1) and SFB914 projects B09 and Z03 to C. Scheiermann, SFB914 project B05 to R.H., SFB654 project C08 to W.S. and H.O., TR128 project B10 and a Heisenberg fellowship to N.K., SFB-TR84 project C08 to L.E.S., C. Schmal and H.H. are supported by BO 3612/2-1. C. Scheiermann holds a European Research Council (ERC) starting grant (635872, CIRCODE). H.O. is a Lichtenberg fellow of the Volkswagen

Foundation. L.E.S. and L.Y. are supported by the Else Kröner Fresenius Foundation (EKFS, 2012_A56 to L.E.S.).

Received: July 2, 2016
Revised: October 24, 2016
Accepted: November 18, 2016
Published: January 10, 2017

REFERENCES

Arjona, A., and Sarkar, D.K. (2005). Circadian oscillations of clock genes, cytolytic factors, and cytokines in rat NK cells. Journal of Immunology *174*, 7618–7624.

Arjona, A., Silver, A.C., Walker, W.E., and Fikrig, E. (2012). Immunity's fourth dimension: approaching the circadian-immune connection. Trends Immunol. *33*, 607–612.

Bollinger, T., Leutz, A., Leliavski, A., Skrum, L., Kovac, J., Bonacina, L., Benedict, C., Lange, T., Westermann, J., Oster, H., and Solbach, W. (2011). Circadian clocks in mouse and human CD4+ T cells. PLoS ONE *6*, e29801.

Bunger, M.K., Wilsbacher, L.D., Moran, S.M., Clendenin, C., Radcliffe, L.A., Hogenesch, J.B., Simon, M.C., Takahashi, J.S., and Bradfield, C.A. (2000). Mop3 is an essential component of the master circadian pacemaker in mammals. Cell *103*, 1009–1017.

Butcher, E.C. (1991). Leukocyte-endothelial cell recognition: three (or more) steps to specificity and diversity. Cell *67*, 1033–1036.

Curtis, A.M., Bellet, M.M., Sassone-Corsi, P., and O'Neill, L.A. (2014). Circadian clock proteins and immunity. Immunity *40*, 178–186.

Cyster, J.G., and Schwab, S.R. (2012). Sphingosine-1-phosphate and lymphocyte egress from lymphoid organs. Annu. Rev. Immunol. *30*, 69–94.

Dibner, C., Schibler, U., and Albrecht, U. (2010). The mammalian circadian timing system: organization and coordination of central and peripheral clocks. Annu. Rev. Physiol. *72*, 517–549.

Esquifino, A.I., Selgas, L., Arce, A., Maggiore, V.D., and Cardinali, D.P. (1996). Twenty-four-hour rhythms in immune responses in rat submaxillary lymph nodes and spleen: effect of cyclosporine. Brain Behav. Immun. *10*, 92–102.

Förster, R., Schubel, A., Breitfeld, D., Kremmer, E., Renner-Müller, I., Wolf, E., and Lipp, M. (1999). CCR7 coordinates the primary immune response by establishing functional microenvironments in secondary lymphoid organs. Cell *99*, 23–33.

Förster, R., Davalos-Misslitz, A.C., and Rot, A. (2008). CCR7 and its ligands: balancing immunity and tolerance. Nat. Rev. Immunol. *8*, 362–371.

Fortier, E.E., Rooney, J., Dardente, H., Hardy, M.P., Labrecque, N., and Cermakian, N. (2011). Circadian variation of the response of T cells to antigen. Journal of Immunology *187*, 6291–6300.

Gasteiger, G., Ataide, M., and Kastenmüller, W. (2016). Lymph node - an organ for T-cell activation and pathogen defense. Immunol. Rev. *271*, 200–220.

Gibbs, J., Ince, L., Matthews, L., Mei, J., Bell, T., Yang, N., Saer, B., Begley, N., Poolman, T., Pariollaud, M., et al. (2014). An epithelial circadian clock controls pulmonary inflammation and glucocorticoid action. Nat. Med. *20*, 919–926.

Girard, J.P., Moussion, C., and Förster, R. (2012). HEVs, lymphatics and homeostatic immune cell trafficking in lymph nodes. Nat. Rev. Immunol. *12*, 762–773.

Haus, E., and Smolensky, M.H. (1999). Biologic rhythms in the immune system. Chronobiol. Int. *16*, 581–622.

Hemmers, S., and Rudensky, A.Y. (2015). The Cell-Intrinsic Circadian Clock Is Dispensable for Lymphocyte Differentiation and Function. Cell Rep. *11*, 1339–1349.

Kawakami, N., Bartholomäus, I., Pesic, M., and Mues, M. (2012). An autoimmunity odyssey: how autoreactive T cells infiltrate into the CNS. Immunol. Rev. *248*, 140–155.

Keller, M., Mazuch, J., Abraham, U., Eom, G.D., Herzog, E.D., Volk, H.D., Kramer, A., and Maier, B. (2009). A circadian clock in macrophages controls inflammatory immune responses. Proc. Natl. Acad. Sci. USA *106*, 21407–21412.

Labrecque, N., and Cermakian, N. (2015). Circadian Clocks in the Immune System. J. Biol. Rhythms *30*, 277–290.

Ley, K., Laudanna, C., Cybulsky, M.I., and Nourshargh, S. (2007). Getting to the site of inflammation: the leukocyte adhesion cascade updated. Nat. Rev. Immunol. *7*, 678–689.

Lo, C.G., Xu, Y., Proia, R.L., and Cyster, J.G. (2005). Cyclical modulation of sphingosine-1-phosphate receptor 1 surface expression during lymphocyte recirculation and relationship to lymphoid organ transit. J. Exp. Med. *201*, 291–301.

Long, J.E., Drayson, M.T., Taylor, A.E., Toellner, K.M., Lord, J.M., and Phillips, A.C. (2016). Morning vaccination enhances antibody response over afternoon vaccination: A cluster-randomised trial. Vaccine *34*, 2679–2685.

Lucas, D., Battista, M., Shi, P.A., Isola, L., and Frenette, P.S. (2008). Mobilized hematopoietic stem cell yield depends on species-specific circadian timing. Cell Stem Cell *3*, 364–366.

Mandl, J.N., Liou, R., Klauschen, F., Vrisekoop, N., Monteiro, J.P., Yates, A.J., Huang, A.Y., and Germain, R.N. (2012). Quantification of lymph node transit times reveals differences in antigen surveillance strategies of naive CD4+ and CD8+ T cells. Proc. Natl. Acad. Sci. USA *109*, 18036–18041.

Massberg, S., and von Andrian, U.H. (2006). Fingolimod and sphingosine-1-phosphate–modifiers of lymphocyte migration. N. Engl. J. Med. *355*, 1088–1091.

Matloubian, M., Lo, C.G., Cinamon, G., Lesneski, M.J., Xu, Y., Brinkmann, V., Allende, M.L., Proia, R.L., and Cyster, J.G. (2004). Lymphocyte egress from thymus and peripheral lymphoid organs is dependent on S1P receptor 1. Nature *427*, 355–360.

Méndez-Ferrer, S., Lucas, D., Battista, M., and Frenette, P.S. (2008). Haematopoietic stem cell release is regulated by circadian oscillations. Nature *452*, 442–447.

Mohawk, J.A., Green, C.B., and Takahashi, J.S. (2012). Central and peripheral circadian clocks in mammals. Annu. Rev. Neurosci. *35*, 445–462.

Moon, J.J., Chu, H.H., Pepper, M., McSorley, S.J., Jameson, S.C., Kedl, R.M., and Jenkins, M.K. (2007). Naive CD4(+) T cell frequency varies for different epitopes and predicts repertoire diversity and response magnitude. Immunity *27*, 203–213.

Muller, W.A. (2011). Mechanisms of leukocyte transendothelial migration. Annu. Rev. Pathol. *6*, 323–344.

Nguyen, K.D., Fentress, S.J., Qiu, Y., Yun, K., Cox, J.S., and Chawla, A. (2013). Circadian gene Bmal1 regulates diurnal oscillations of Ly6C(hi) inflammatory monocytes. Science *341*, 1483–1488.

Pham, T.H., Okada, T., Matloubian, M., Lo, C.G., and Cyster, J.G. (2008). S1P1 receptor signaling overrides retention mediated by G alpha i-coupled receptors to promote T cell egress. Immunity *28*, 122–133.

Phillips, A.C., Gallagher, S., Carroll, D., and Drayson, M. (2008). Preliminary evidence that morning vaccination is associated with an enhanced antibody response in men. Psychophysiology *45*, 663–666.

Scheiermann, C., Kunisaki, Y., Lucas, D., Chow, A., Jang, J.E., Zhang, D., Hashimoto, D., Merad, M., and Frenette, P.S. (2012). Adrenergic nerves govern circadian leukocyte recruitment to tissues. Immunity *37*, 290–301.

Scheiermann, C., Kunisaki, Y., and Frenette, P.S. (2013). Circadian control of the immune system. Nat. Rev. Immunol. *13*, 190–198.

Shiow, L.R., Rosen, D.B., Brdicková, N., Xu, Y., An, J., Lanier, L.L., Cyster, J.G., and Matloubian, M. (2006). CD69 acts downstream of interferon-alpha/beta to inhibit S1P1 and lymphocyte egress from lymphoid organs. Nature *440*, 540–544.

Silver, A.C., Arjona, A., Hughes, M.E., Nitabach, M.N., and Fikrig, E. (2012a). Circadian expression of clock genes in mouse macrophages, dendritic cells, and B cells. Brain Behav. Immun. *26*, 407–413.

Silver, A.C., Arjona, A., Walker, W.E., and Fikrig, E. (2012b). The circadian clock controls toll-like receptor 9-mediated innate and adaptive immunity. Immunity *36*, 251–261.

Springer, T.A. (1994). Traffic signals for lymphocyte recirculation and leukocyte emigration: the multistep paradigm. Cell *76*, 301–314.

Sun, Y., Yang, Z., Niu, Z., Peng, J., Li, Q., Xiong, W., Langnas, A.N., Ma, M.Y., and Zhao, Y. (2006). MOP3, a component of the molecular clock, regulates the development of B cells. Immunology *119*, 451–460.

Vestweber, D., and Blanks, J.E. (1999). Mechanisms that regulate the function of the selectins and their ligands. Physiol. Rev. *79*, 181–213.

von Andrian, U.H., and Mempel, T.R. (2003). Homing and cellular traffic in lymph nodes. Nat. Rev. Immunol. *3*, 867–878.

Wagner, D.D., and Frenette, P.S. (2008). The vessel wall and its interactions. Blood *111*, 5271–5281.

Yu, X., Rollins, D., Ruhn, K.A., Stubblefield, J.J., Green, C.B., Kashiwada, M., Rothman, P.B., Takahashi, J.S., and Hooper, L.V. (2013). TH17 cell differentiation is regulated by the circadian clock. Science *342*, 727–730.

Immunity, Volume *46*

Supplemental Information

Lymphocyte Circadian Clocks Control Lymph Node Trafficking and Adaptive Immune Responses

David Druzd, Olga Matveeva, Louise Ince, Ute Harrison, Wenyan He, Christoph Schmal, Hanspeter Herzel, Anthony H. Tsang, Naoto Kawakami, Alexei Leliavski, Olaf Uhl, Ling Yao, Leif Erik Sander, Chien-Sin Chen, Kerstin Kraus, Alba de Juan, Sophia Martina Hergenhan, Marc Ehlers, Berthold Koletzko, Rainer Haas, Werner Solbach, Henrik Oster, and Christoph Scheiermann

SUPPLEMENTAL INFORMATION

Figure S1

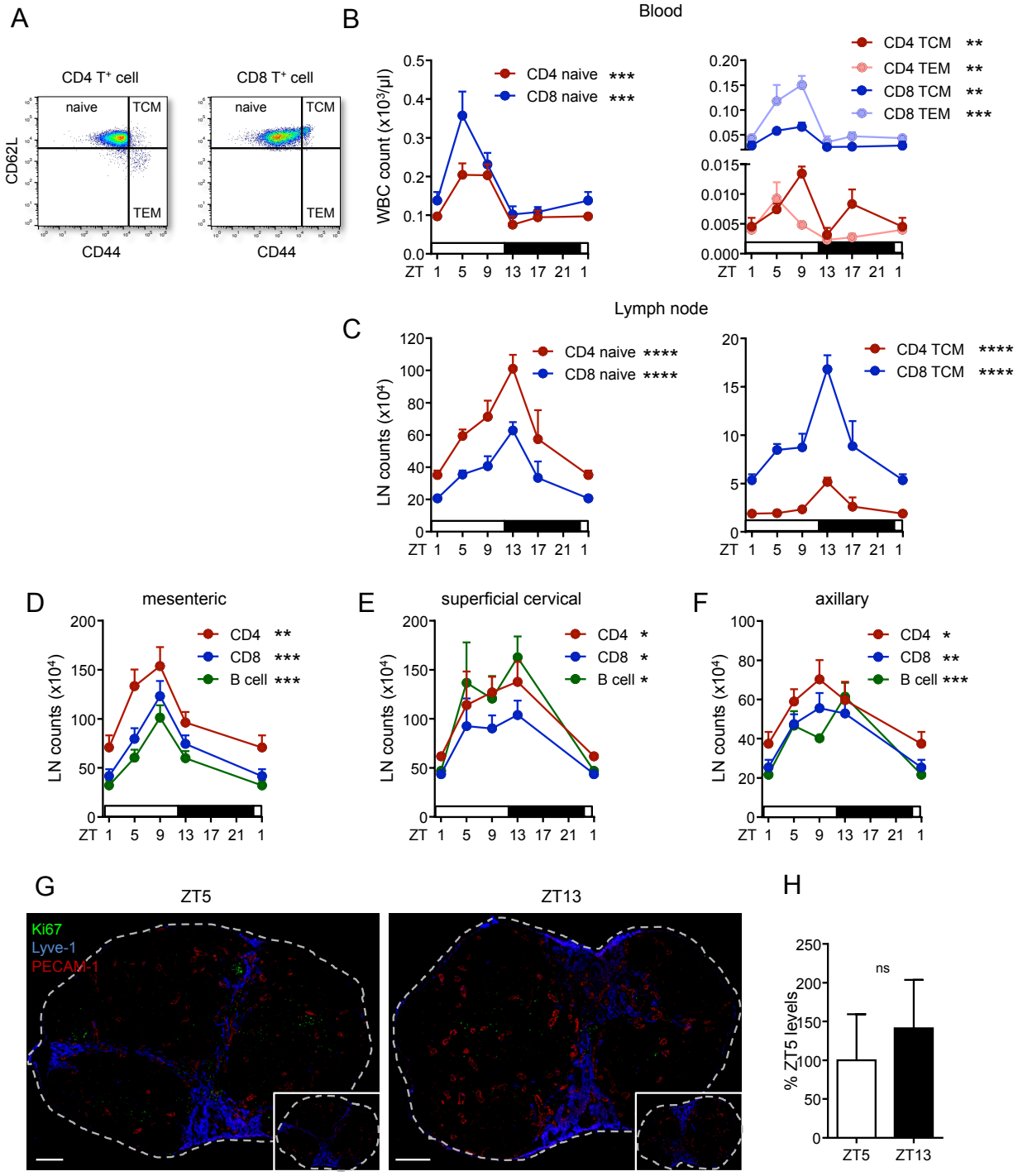

Figure S1, related to Figure 1

Oscillatory T lymphocyte subpopulations in blood and lymph node

(A-C) Gating strategy (gated on live cells) **(A)** and counts of naïve, central memory (TCM) and effector memory (TEM) CD4 and CD8 T lymphocytes in **(B)** blood (n=3-5 mice) and **(C)** lymph node (n= 6-18 mice); one-way ANOVA. **(D-F)** Counts of CD4 and CD8 T cells and B cells in **(D)** mesenteric lymph node (n=7-11 mice) **(E)** superficial cervical lymph node (n=4-7 mice) and **(F)** axillary lymph node (n=7 mice); one-way ANOVA. **(G)** Images of lymph node sections harvested at ZT5 and ZT13 and stained with antibodies directed against Ki67, PECAM-1, and Lyve-1. Inset: isotype antibody-stained control sections. Scale bars: 200 μm. **(H)** Quantification of $Ki67^+$ cells per lymph node section; n=4-5 mice. *p<0.05, **p<0.01, ***p<0.001, ****p<0.0001.

Figure S2

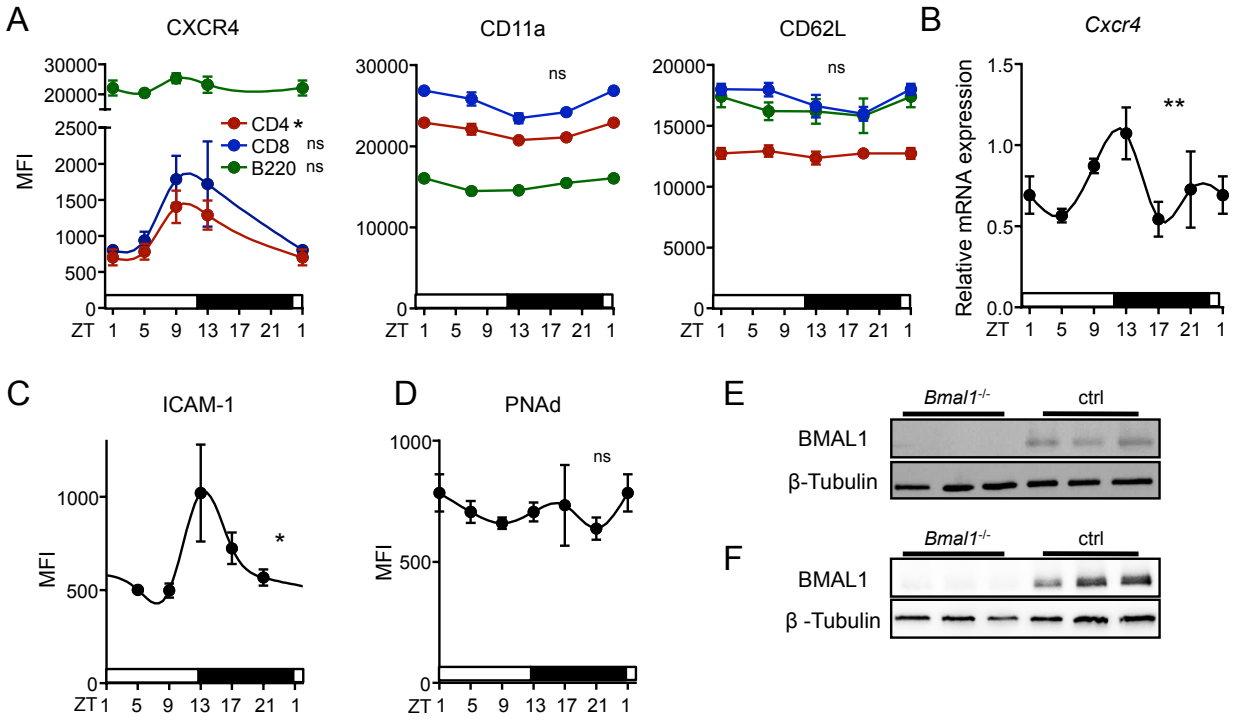

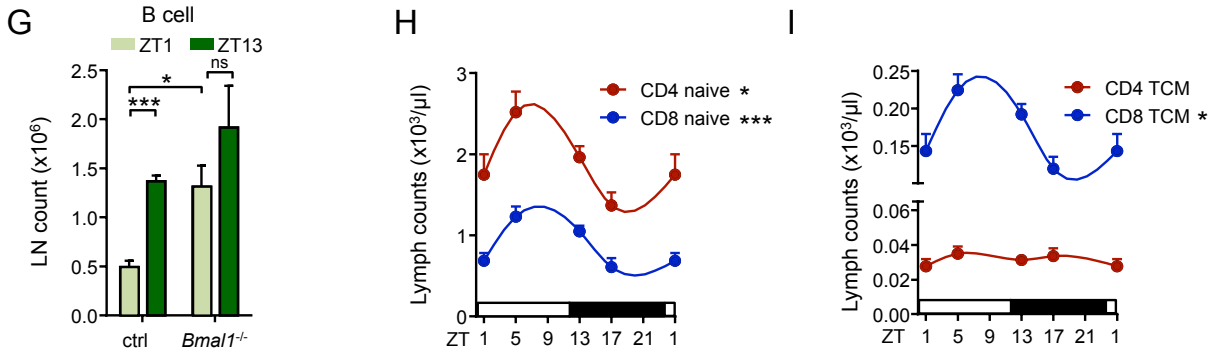

J

Time	ZT1	ZT7	ZT13	ZT21
Lymph volume (µl)	72 ± 5	70 ± 5	68 ± 4	79 ± 4
Lymph flow (µl/min)	1.2 ± 0.1	1.2 ± 0.1	1.1 ± 0.1	1.3 ± 0.1

Figure S2, related to Figures 2, 3 and 4

Oscillations of leukocyte promigratory factors and numbers

(A) Oscillations in protein surface expression on lymphocyte subpopulations in lymph nodes; CXCR4, CD11a, CD62L; n=3-5 mice, one-way ANOVA; MFI, mean fluorescence intensity. **(B)** Q-PCR analysis of LN *Cxcr4* over 24h; n=3-5 mice, one-way ANOVA. **(C-D)** Quantification of expression of ICAM-1 **(C)** and PNAd **(D)** on HEV over 24h in constant darkness (CT, circadian time: the corresponding light and dark phase are indicated); n=3 mice, one-way ANOVA. **(E)** Amount of BMAL1 protein in isolated splenic T cells from T cell specific *Bmal1*$^{-/-}$ and control animals; n = 3 mice, each lane represents an individual animal. **(F)** Amount of BMAL1 protein in isolated splenic B cells from B cell specific *Bmal1*$^{-/-}$ and control animals, each lane represents a technical replicate. **(G)** Lymph node B cell counts in control and B-cell-specific *Bmal1*$^{-/-}$ mice; n=3-4 mice, unpaired student's t-test. **(H-I)** Counts of naïve and central memory (TCM) CD4 and CD8 T lymphocytes in lymph; n=5-17 mice, one-way ANOVA. **(J)** Harvested lymph volume and flow rate over 24h; n=7-22 mice. *p<0.05, **p<0.01, ***p<0.001.

Figure S3

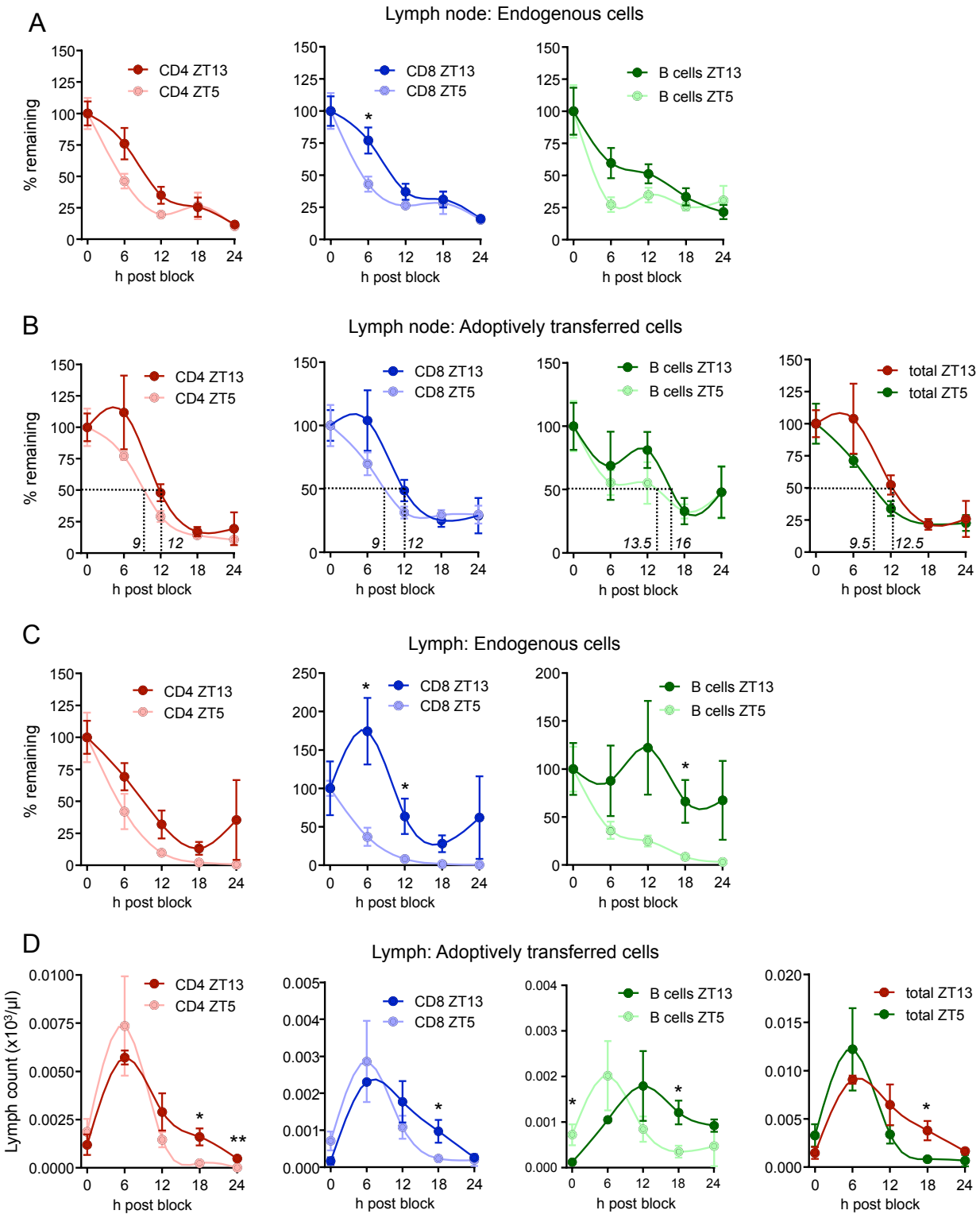
A
Lymph node: Endogenous cells
CD4 ZT13
CD4 ZT5
CD8 ZT13
CD8 ZT5
B cells ZT13
B cells ZT5
% remaining
h post block
B
Lymph node: Adoptively transferred cells
total ZT13
total ZT5
9
12
13.5
16
9.5
12.5
C
Lymph: Endogenous cells
D
Lymph: Adoptively transferred cells
Lymph count (x10³/µl)

Figure S3, related to Figure 4

Analysis of oscillations in lymph node half life

Change in cellular numbers (in % **(A-C)**) or absolute numbers **(D)** of endogenous **(A** and **C)** and adoptively transferred **(B** and **D)** leukocytes in lymph node and lymph over 24h after block of leukocyte homing. Lymph node: n= 3-10 mice; lymph: n=3-6 mice, unpaired student's t-test. *$p<0.05$, **$p<0.01$.

Figure S4

For the sake of simplicity, it was assumed that both homing and egress rhythms follow a sinusoidal oscillation with a certain amplitude and phase. The individual phases were termed Φ_h and Φ_e, respectively.
Let $x(t)$ be the time-dependent lymphocyte count in the lymph node:

$$dx(t)/dt = g(t) - l(t) \quad (1)$$

Here, the time-dependent gain rate is represented by $g(t)$ and can be summarised as a non-negative sinusoidal function of the form:

$$g(t) = A(1 + \sin(\omega t + \Phi_h)) \quad (2)$$

where A is amplitude and ω is angular frequency. The time-dependent loss rate is represented by $l(t)$ and can be replaced by a non-negative sinusoidal function of the form:

$$l(t) = d(1 + \sin(\omega t + \Phi_e))\, x(t) \quad (3)$$

where d is decay rate and other nomenclature remains the same.

Using these formulae, a model for circadian homing with the egress replaced with a simple exponential decay rate can be summarised as:

$$dx(t)/dt = A(1 + \sin(\omega t + \Phi_h)) - dx(t) \quad (4)$$

A model for circadian egress with a fixed gain rate can be summarised as:

$$dx(t)/dt = A - d(1 + \sin(\omega t + \Phi_e))\, x(t) \quad (5)$$

A model where both homing and egress oscillate can be summarised as:

$$dx(t)/dt = A(1 + \sin(\omega t + \Phi_h)) - d(1 + \sin(\omega t + \Phi_e))\, x(t) \quad (6)$$

Model parameters were estimated by fitting to time series data obtained under steady state and blocked homing conditions. Time series data obtained under a blocked egression was spared from the fitting and taken as a cross-validation. Comparisons of modelled and actual data in steady state conditions are shown in Figure 4G (total cell count) and below (individual subsets).

The relative quality of the models given our set of data was tested by means of the Akaike information criterion (AIC), using the formula commonly used for regression models. Its value can be given by:

$$AIC = N \ln(X^2/N) + 2K \quad (7)$$

where N is the number of data points, K is the number of parameters plus one, and X^2 is the residual sum of squares. Models with smaller numbers of AIC values are assumed to outperform those with higher values.

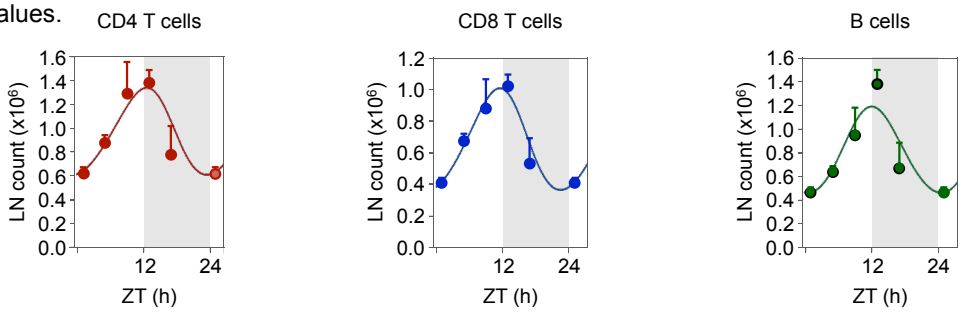

Figure S4, related to Figure 4

Mathematical modeling of cellular oscillations in lymph nodes

Formulas and fits for optimal modeling parameter sets (curves) vs. actual data sets (points) for steady-state oscillations of CD4 and CD8 T cells and B cells using the dual oscillation mathematical model that incorporates rhythmic homing to LNs and rhythmic egress from LNs. The ZT1 time point has been double-plotted to facilitate viewing.

Figure S5

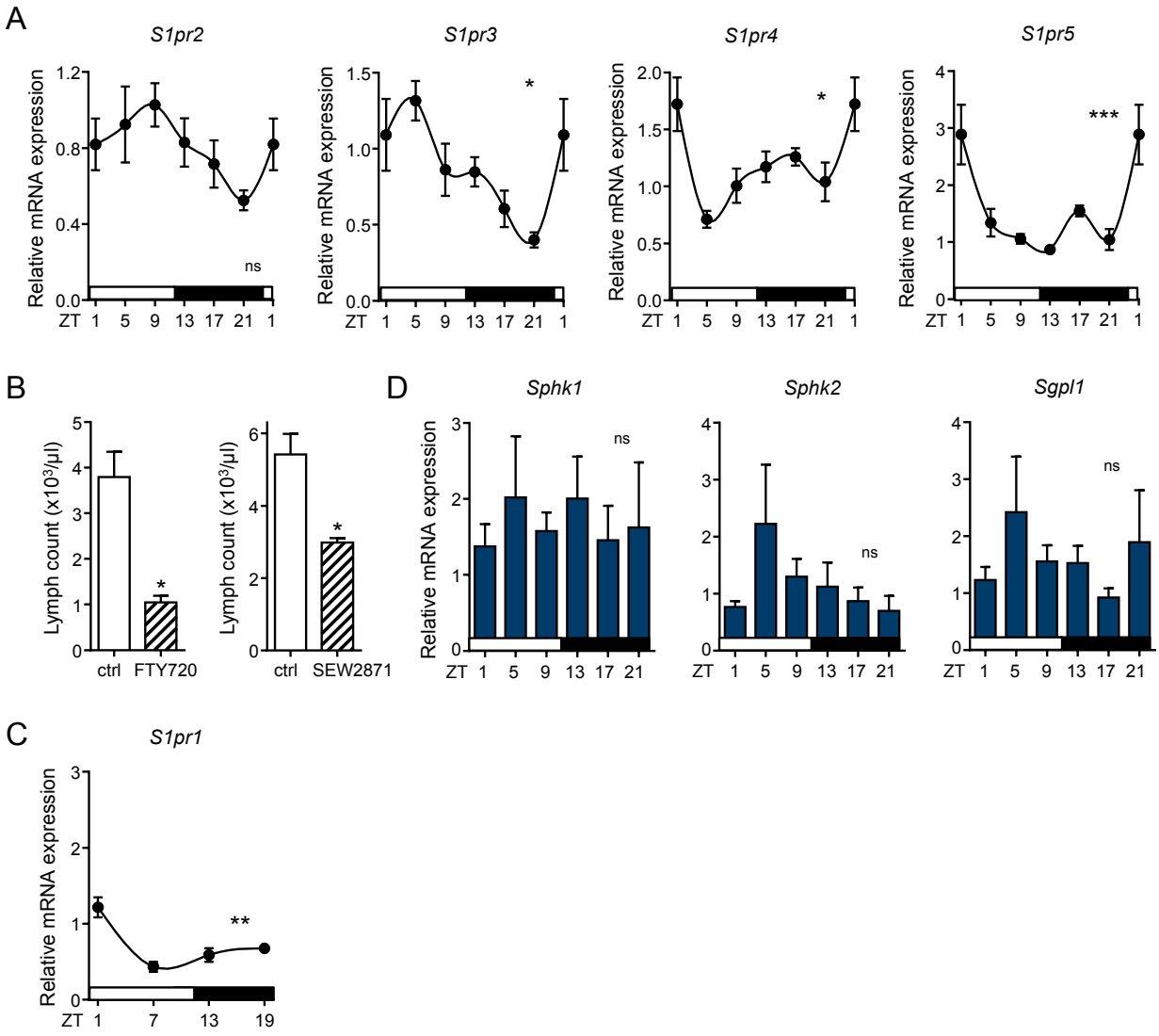
A
S1pr2
S1pr3
S1pr4
S1pr5
Relative mRNA expression
ns
*
*
***
ZT 1 5 9 13 17 21 1
B
Lymph count (x10³/µl)
ctrl FTY720
ctrl SEW2871
D
Sphk1
Sphk2
Sgpl1
ns
ns
ns
ZT 1 5 9 13 17 21
C
S1pr1
**
ZT 1 7 13 19

Figure S5, related to Figure 5

Diurnal expression profiles of *S1pr* genes

(A) Q-PCR analysis of LN *S1pr2*, *S1pr3*, *S1pr4* and *S1pr5* over 24h; n=3-5 mice, one-way ANOVA. **(B)** Lymph counts in control animals or animals treated with FTY720 or SEW2871; n=3-6 mice, unpaired student's t-test. **(C)** Q-PCR analysis of *S1pr1* in CD4 T cells isolated from *S1pr1*$^{+/-}$*xCd4-cre* mice over 24h; n=3 mice, one-way ANOVA. **(D)** Q-PCR analysis of LN Sphingosine kinase 1 and 2 (*Sphk1* and *Sphk2*) and Sphingosine-1-phosphate lyase *(Sgpl1)* over 24h; n=3-5 mice, one-way ANOVA. *p<0.05, **p<0.01, ***p<0.001.

Figure S6

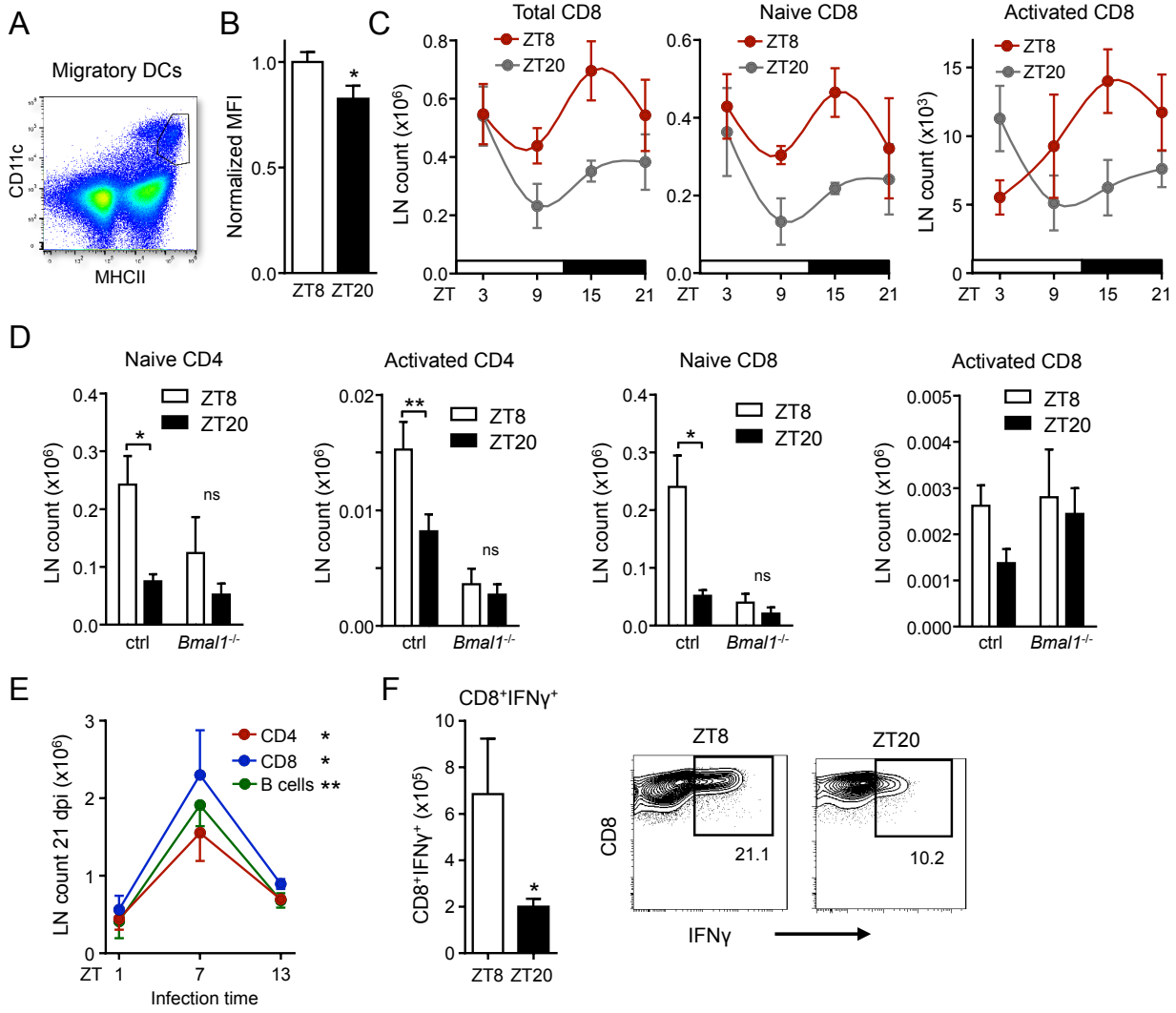
A
Migratory DCs
CD11c
MHCII
B
Normalized MFI
ZT8 ZT20
C
Total CD8
Naive CD8
Activated CD8
ZT8
ZT20
LN count (x10^6)
LN count (x10^3)
ZT 3 9 15 21
D
Naive CD4
Activated CD4
Naive CD8
Activated CD8
LN count (x10^6)
ctrl
Bmal1-/-
ns
E
CD4 *
CD8 *
B cells **
LN count 21 dpi (x10^6)
Infection time
F
CD8+IFNγ+
CD8+IFNγ+ (x10^5)
ZT8
ZT20
CD8
IFNγ
21.1
10.2

Figure S6, related to Figure 6

Diurnal rhythmicity in experimental autoimmune encephalomyelitis (EAE)

(A) Gating strategy (gated on live singlet cells) of migratory DCs. (**B**) Proliferation of MOG-specific T cells as analyzed by *in vivo* immunization of mice at ZT8 and ZT20, followed by dye-dilution analyses after re-stimulation with the antigen in culture; n=10 mice, unpaired student's t-test. **(C)** Diurnal profiles of inguinal lymph node counts of total CD8 T cells, naïve CD8 T cells, and activated CD8 T cells on day 2 after EAE induction; n=4 mice. Black and white bars indicate the dark and light periods, respectively **(D)** Naïve and activated CD4 and CD8 T cell counts in inguinal lymph nodes sampled at ZT15 on the second day after EAE induction; n=4-5 mice, unpaired student's t-test. **(E)** Lymph node counts of mice that were infected at different times of the day (ZT1, ZT7 or ZT13) with *Helicobacter pylori* and harvested at one time 21 days post infection (dpi); n=4 mice, one-way ANOVA. **(F)** Pulmonary $CD8^{+}IFN\gamma^{+}$ T cells of mice infected with influenza A virus at different times of the day (ZT8 and ZT20). Lungs were harvested 8 dpi and infiltrating T cells were enumerated and IFNγ production was assessed by flow cytometry; n=4 mice, Mann-Whitney test. *$p<0.05$, **$p<0.01$.

Primers	Sequence	Annealing(°C)
Bmal1_F	AGA GGT GCC ACC AAC CCA TA	62
Bmal1_R	TGA GAA TTA GGT GTT TCA GTT CGT CAT	
Bmal1_F	CCT AAT TCT CAG GGC AGC AGA T	60
Bmal1_R	TCC AGT CTT GGC ATC AAT GAG T	
Clock_F	CAA AAT GTC ACG AGC ACT TAA TGC	62
Clock _R	ATA TCC ACT GCT GGC CTT TGG	
Per1_F	TGA GAG CAG CAA GAG TAC AAA CTC A	60
Per1_R	CTC GCA CTC AGG AGG CTG TAG	
Per2_F	GTC CAC CTC CCT GCA GAC AA	60
Per2_R	TCA TTA GCC TTC ACC TGC TTC AC	
Cry1_F	CTC GGG TGA GGA GGT TTT CTT	62
Cry1_R	GAC TTC CTC TAC CGA GAG CTT CAA	
Nr1d1_F	GAT AGC TCC CCT TCT TCT GCA TCA TC	60
Nr1d1_R	TTC CAT GGC CAC TTG TAG ACT TC	
Nr1d1_F	AGC TCA ACT CCC TGG CAC TTA C	60
Nr1d1_R	CTT CTC GGA ATG CAT GTT GTT C	
Dbp_F	AAT GAC CTT TGA ACC TGA TCC CGC T	60
Dbp_R	GCT CCA GTA CTT CTC ATC CTT CTG T	
S1pr1_F	CGG TGT AGA CCC AGA GTC CT	64
S1pr1_R	AGC AGC AGA TGA GAA TGA AC	
S1pr2_F	ATG GGC GGC TTA TAC TCA GAG	60
S1pr2_R	GCG CAG CAC AAG ATG ATG AT	
S1pr3_F	TTC CCG ACT GCT CTA CCA TC	62
S1pr3_R	CCA ACA GGC AAT GAA CAC AC	
S1pr4_F	TGC GGG TGG CTG AGA GTG	62
S1pr4_R	TAG GAT CAG GGC GAA GAC C	
S1pr5_F	CTT AGG ACG CCT GGA AAC C	62
S1pr5_R	CCC GCA CCT GAC AGT AAA TC	
Ccr7_F	TCA TTG CCG TGG TGG TAG TCT TCA	62
Ccr7_R	ATG TTG AGC TGC TTG CTG GTT TCG	
Cxcr4_F	TCA GTG GCT GAC CTC CTC TT	60
Cxcr4_R	CTT GGC CTT TGA CTG TTG GT	
Ccl21_F	ACA GCG GCC TCC AGA AGA ACA GCG G	64
Ccl21_R	CGT GAA CCA CCC AGC TTG A	
Gapdh_F	TGT GTC CGT CGT GGA TCT GA	60
Gapdh_R	CCT GCT TCA CCA CCT TCT TGA	
Eef1a_F	TGC CCC AGG ACA CAG AGA CTT CA	60
Eef1a_R	AAT TCA CCA ACA CCA GCA GCA A	
Sphk1_F	GAAGACCTGCTCATCAACTGC	60
Sphk1_R	GTGCCCACTGTGAAACGAA	
Sphk2_F	TAGATGGGGAGTTAGTGGAGTATG	60
Sphk2_F	TGCTTTTAGGCTCGTTCAGG	
Sgpl1_F	TGATGGCCTGCAAAGCTT	60
Sgpl1_R	GCCACAATTTCTGGAGTTTTGA	
Il2_F	AACCTGAAACTCCCCAGGAT	60
Il2_R	CGCAGAGGTCCAAGTTCATC	

Q-PCR primer sequences, related to Figure 2, 3, 5, 6, S2, S5

Movie S1

Movie showing the circadian migration of lymphocytes through lymph nodes. At night onset, increased homing due to higher amounts of lymphocyte CCR7 leads to enhanced lymphocyte counts in the lymph node. During the day, higher *S1pr1* expression induces the egression of lymphocytes into efferent lymph.

SUPPLEMENTAL EXPERIMENTAL PROCEDURES

Antibodies

Antibodies targeting the following antigens were used: CD3e (clone 145-2C11; Biolegend), CD3 (17A2; Biolegend), CD4 (GK1.5; Biolegend), CD8a (53-6.7; Biolegend), CD16/32 (2.4G2; BD Biosciences), CD44 (IM7; Biolegend), CD45 (30-F11; Biolegend), CD62L (MEL-14; Biolegend), B220 (RA3-6B2; Biolegend), NK1.1 (PK136; Biolegend), Gr-1 (RB6-8C5, Biolegend), CD11b (M1/70; Biolegend), CD11c (N418; Biolegend), MHCII I-A/I-E (M5/114.15.2, Biolegend); CCR7 (4B12; Biolegend), CXCR4 (L276F12; Biolegend), CD11a (M17/4; Biolegend), IL-17A (TC11-18H10, BD Horizon), CD49d (R1-2, Biolegend), Ki67 (SolA15; eBioscience), PECAM-1 (Mec13.3; Biolegend), Lyve-1 (ALY7; eBioscience), CCL21 (goat anti-mouse polyclonal; R&D Systems), ICAM-1 (YN1/1.7.4; Biolegend), PNAd (MECA-79, Biolegend), blocking antibodies against CD49d (PS/2) and CD11a (M17/4; both BioXCell), BMAL1 (NB 100-2288; Novus Biologicals), beta-tubulin (ab6046; Abcam).

Mass spectrometry analyses

Proteins of 20 µL sample matrix were precipitated by adding 200 µL methanol including D-erythro-sphingosine-1-phosphate C17 base (860641P, Avanti Polar Lipids) as internal standard. After centrifugation the supernatant was used for the analysis of S1P by liquid chromatography mass spectrometry (LC-MS/MS) analyses with a 1200 SL HPLC system (Agilent) coupled to a 4000QTRAP tandem mass spectrometer (AB Sciex). Separation was achieved with a Zorbax SB-C18, particle size 3.5 µm, 150 mm × 2.1 mm HPLC column (Agilent) and water with 0.1% formic acid as mobile phase A and methanol/ isopropanol (1:1) with 0.1% formic acid as mobile phase B. A gradient elution was used for optimal separation from 60% B to 80% B within 7 minutes. After column cleaning at 100% B for 1 minute, the gradient was equilibrated for 2.5 min at 60% B before the next injection. The LC-MS/MS system operated in positive electrospray ionization with electron voltage of 5500V at 400 °C. Auxiliary gas was set to 50 psi and 60 psi was used for nebulizer gas. Curtain gas was set to 30 psi and collision gas was set to 8 psi. Mass transitions and individual energies (declustering potential, collision energy, collision cell exit potential) were optimized by direct infusion and set as follows: m/z 380.2→264.2 (66, 23, 18) and 380.2→82.1 (66, 49, 6) for S1P and 366.2→250.2 (61, 23, 18) and 366.2→82.0 (61, 45, 6) for internal standard. Mass transitions were detected in multiple reaction monitoring mode with a dwell time of 100 ms. Quantification was achieved by standard calibrating curves prepared from D-erythro-sphingosine-1-phosphate C18:1 base (860492P, Avanti Polar Lipids) at different concentration points in the range from 0.005 to 0.5 µmol/L.

Western blotting

To obtain total cell lysates, MACS-purified T cells were incubated with RIPA buffer (150 mM NaCl; 50 mM Tris-HCl, 0.1 % SDS, 0.5 % Na-Dox, 0.1 % SDS, 1 % NP40, 1 mM EDTA, and proteinase inhibitor). Nuclei were pelleted in a microfuge at 14,000 x g for 15 min, and the supernatant was used as the cytoplasm fraction. Cell lysates were normalized by measuring total protein concentrations using the Pierce BCA Protein Assay Kit (Thermo Scientific) according to the manufacturer's protocol. Proteins were separated on a 10 % SDS-PAGE and transferred to PVDF membranes (Roche). Membranes were blocked in 5 % milk powder for 1 h and then probed with anti-BMAL1 antibody (1:2000 in 5 % milk-TBS; NB 100-2288, Novus Biologicals, Littleton, USA) overnight at 4 °C. Anti-β-Tubulin antibody (Abcam) was used for normalisation. HRP-conjugated anti-rabbit or anti-mouse IgGs were used as secondary antibodies. Proteins were visualized by enhanced chemiluminescence (Thermo, No. 34080) and a Fusion SL Image Acquisition System (Vilber Lourmat).

Histology

Mice were perfused intracardially with ice-cold PBS followed by fixation with 4% paraformaldehyde (PFA) for 10 minutes. Spinal cords were post-fixed overnight and then dissected from the spinal canal. Paraffin embedded 10-µm transverse sections of the lumbar spinal cord were stained for total myelin with Luxol Fast Blue Stain/ Cresyl Echt Violet (Abcam) according to the manufacturer's instructions, dehydrated, cleared with xylene, and mounted for microscopy. Images of lumbar spinal cord were taken at levels L1/2, L3/4 and L5/6 for each mouse and demyelinated areas measured using ImageJ software (National Institutes of Health).

Quantitative real-time PCR

RNA was extracted using RNeasy Plus Mini Kit (Qiagen) or with TRIzol reagent (Life Technologies), in accordance with the manufacturers' instructions. Reverse transcription was carried out using the High Capacity cDNA Reverse Transcription Kit (Applied Biosystems), in accordance with the manufacturer's instructions. Q-PCR was performed with SYBR GREEN on a StepOnePlus Real-Time PCR System (Applied Biosystems). A primer concentration of 0.5µM was found to be optimal in all cases. The sequences of the oligonucleotides used are included in the Supplemental Experimental Procedures. The PCR protocol consisted of one cycle at 95 °C (10 min) followed by 40 cycles of 95 °C (15 s) and 60-64 °C (1 min). Expression of glyceraldehyde-3-phosphate dehydrogenase (GAPDH) was generally used as a standard. For EAE experiments Q-PCR was conducted with the GoTaq Q-PCR Master Mix (Promega) and a CFX96 Real-Time PCR Detection System (Bio-Rad) according to the manufacturer's instructions, along with gene-specific primers. Eef1a was used as reference gene. Relative quantification was performed using the ΔΔCT method.

T-cell proliferation analyses

Spleens were harvested from mice 10 days after EAE immunization. CD3+ T cells were negatively selected using the Pan T Cell Isolation Kit II (Miltenyi Biotec) and labelled with a proliferation dye (CellTrace™ Violet Cell Proliferation Kit, Life Technologies). T-cell depleted splenocytes (1×10^5/well) isolated from EAE mice were

cultured in the presence or absence of the MOG peptide (10 µg/ml) or irrelevant peptide (ovalbumin) (10 µg/ml) or no antigen at 37℃ in 5% CO2 for 1 h. CD3+ T cells were co-cultured with antigen-pulsed splenocytes at 37°C in 5% CO2 for 3 days RPMI medium 1640 supplemented with 10% FCS, 10mM HEPES and 55µM beta-mercaptoethanol in 96-well flat-bottom plates, at 2×10^5 cells per well.

Helicobacter pylori infection

Mice were infected orogastrically at ZT1, ZT7 and ZT13 with the H. pylori strain PMSS1wt with a dose of 109 bacteria. Animals were sacrificed after 3 weeks and LN cellularity was analyzed by flow cytometry.

Influenza A virus infection

Female 8-10 week old C57B/6 (CD45.1+) mice were intranasally infected with 100 plaque forming units (pfu) of Influenza A virus (strain A/Puerto Rico/8/1934 H1N1) at ZT8 and ZT20. Animals were sacrificed on day 8 post infection and lymphocyte infiltration and activation was assessed in lung tissue homogenates by flow cytometry. Animal experiments were approved by the local animal ethics committee (LAGeSo).